Ribosome association inhibits stress-induced gene mRNA localization to stress granules

Noah S. Helton,[1,2] Benjamin Dodd,[1,2] and Stephanie L. Moon[1,2]

[1]Department of Human Genetics, University of Michigan, Ann Arbor, Michigan 48109, USA; [2]Center for RNA Biomedicine, University of Michigan, Ann Arbor, Michigan 48109, USA

The integrated stress response (ISR) is critical for resilience to stress and is implicated in numerous diseases. During the ISR, translation is repressed, stress-induced genes are expressed, and mRNAs condense into stress granules. The relationship between stress granules and stress-induced gene expression is unclear. We measured endogenous stress-induced gene mRNA localization at the single-molecule level in the presence or absence of small molecule translation inhibitors. Reducing ribosome association increases the localization of stress-induced gene mRNAs to stress granules, whereas increasing ribosome association inhibits their localization to stress granules. The presence of upstream open reading frames (uORFs) in mRNA reporters reduces their localization to stress granules in a ribosome-dependent manner. Furthermore, a single initiating ribosome blocks stress granule formation and inhibits mRNA association with preformed stress granules. Thus, uORF-mediated ribosome association inhibits stress-induced gene mRNA localization to stress granules, suggesting a new role for uORFs in limiting RNA condensation.

[*Keywords*: stress granules; translation; upstream open reading frame; integrated stress response; condensate; ATF4; GADD34; ribosome; RNA localization; stress-induced genes]

Supplemental material is available for this article.

Received April 3, 2025; revised version accepted April 4, 2025.

The integrated stress response (ISR) signaling pathway orchestrates the response and adaptation to cellular stress (Pakos-Zebrucka et al. 2016; Costa-Mattioli and Walter 2020). The ISR is induced when stress-sensing kinases phosphorylate eIF2α, suppressing ternary complex formation and translation initiation (Scorsone et al. 1987; Rowlands et al. 1988; Chen et al. 1991; Dever et al. 1992; Wek et al. 1995; Brostrom and Brostrom 1998). Global translation suppression results in stress granule assembly and stress-induced gene mRNA translation (Nover et al. 1983, 1989; Hinnebusch 1997; Kedersha et al. 1999; Harding et al. 2000; Tourrière et al. 2003). Stress granules form via multivalent RNA–RNA, RNA–protein, and protein–protein interactions (e.g., those mediated by G3BP stress granule assembly factors) when mRNAs are released from polysomes (Bounedjah et al. 2014; Van Treeck et al. 2018; Guillén-Boixet et al. 2020; Sanders et al. 2020; Yang et al. 2020). Constitutively expressed transcripts that assemble into stress granules are translationally repressed (Moon et al. 2019; Baymiller and Moon 2023). At the same time, stress-induced genes translate during stress in part through *cis*-acting 5′ untranslated region features such as upstream open reading frames (uORFs) that promote translation when ternary complex is limited (Abastado et al. 1991; Vattem and Wek 2004; Andreev et al. 2015). Translation of key stress-induced genes via uORFs, such as the transcription factor *ATF4* and the translation derepressor *GADD34*, is critical for cellular stress adaptation and survival (Novoa et al. 2003; Han et al. 2013). Specifically, ATF4 upregulates stress-induced genes including genes involved in translation, autophagy, or stress-specific responses (Han et al. 2013; Neill and Masson 2023). GADD34 (in complex with protein phosphatase 1) derepresses translation by dephosphorylating P-eIF2α to resolve the ISR (Novoa et al. 2003). Other stress-induced genes (e.g., *HSP70* and *JUN*) aid in maintaining proteostasis during stress (Hu et al. 2022) or promote cell fate pathways after stress (Behrens et al. 1999; Wisdom et al. 1999). Therefore, stress-induced genes are critical for gene expression reprogramming at the transcriptional and post-transcriptional levels during the ISR.

Corresponding author: smslmoon@umich.edu

Article published online ahead of print. Article and publication date are online at http://www.genesdev.org/cgi/doi/10.1101/gad.352899.125. Freely available online through the *Genes & Development* Open Access option.

Although the ISR is associated with cellular resilience in response to acute, low-level stress, a chronic and/or severe ISR is paradoxically associated with cell death and disease states including cancers (Costa-Mattioli and Walter 2020; Ge et al. 2022), neurodevelopmental disorders (Pae et al. 2005; Moon and Parker 2018; Jia et al. 2022), and neurodegenerative diseases (Ishimura et al. 2016; Costa-Mattioli and Walter 2020; Asadi et al. 2021; Spaulding et al. 2021; English et al. 2022). Modulation of the ISR holds promise for the identification of new therapeutic targets, as many drugs that inhibit the ISR are in clinical trials or are FDA-approved for treatment of cancers and neurodegenerative diseases (Tsuchida et al. 2017; Marlin et al. 2022; Tang et al. 2022; Lines et al. 2023; Sun et al. 2023). However, ISR inhibition can also be detrimental to cell viability and in disease contexts (Boyce et al. 2005; Han et al. 2013; Ishimura et al. 2016; Moon et al. 2018). Thus, a better understanding of the molecular mechanisms of how cells reprogram gene expression during the ISR to promote cellular resilience and adaptation to stress will suggest novel therapeutic strategies for a wide range of diseases.

Although stress granules and stress-induced gene expression are temporally linked, an underexplored area in the field is the relationship between these two branches of the ISR. A general model of stress granules is that they are sites of translational suppression; thus, an a priori assumption is that stress-induced gene mRNAs likely evade stress granule sequestration. The release of mRNAs from polysomes is necessary for stress granule assembly (Kedersha et al. 2000; Markmiller et al. 2018), suggesting a negative connection between translating mRNAs, which would be stress-induced, and stress granules. Furthermore, live-cell single-mRNA imaging demonstrated that translating mRNAs transiently interact with stress granules, whereas nontranslating mRNAs can stably interact with stress granules where they are prevented from re-entering the translating pool (Moon et al. 2019, 2020). Additionally, 60S subunits and 80S ribosomes are depleted in stress granules compared with the surrounding cytoplasm, whereas 40S and preinitiation complexes are enriched in stress granules (Kedersha et al. 2002; Moon et al. 2020; Guo et al. 2024), suggesting that translation is suppressed inside of stress granules. Finally, analysis of the nascent proteome during arsenite stress revealed a negative correlation between translating mRNAs and mRNAs enriched in stress granules in human cells (Baron et al. 2019). Similarly, a recent study demonstrated that highly translated and newly transcribed mRNAs were generally excluded from stress-induced condensates isolated by sedimentation in budding yeast (Glauninger et al. 2024). Together, these data suggest that actively translating mRNAs, such as key stress-induced genes, are not sequestered within stress granules. However, most studies to date have relied on correlation analyses of RNA sequencing data sets derived from purified, biochemically stable particles that do not fully represent intact, dynamic stress granules. Thus, there is a need to directly investigate whether and how stress-induced gene mRNAs evade condensation within stress granules.

Although there is a significant amount of evidence that indicates that translating mRNAs are excluded from stress granules, multiple lines of evidence suggest that stress granules may regulate stress-induced gene expression. First, qualitative, fixed-cell microscopy assays showed that endogenous stress-induced gene mRNAs can colocalize with stress granules (Kedersha and Anderson 2002; Stöhr et al. 2006; Adjibade et al. 2015). Second, live-cell single-molecule microscopy with nascent chain translation reporters harboring the 5′ untranslated region of *ATF4* revealed rare instances of increased nascent chain signal on the reporter construct that colocalized with a stress granule over time (Mateju et al. 2020). The results of this study suggest that translation initiation and elongation can occur within stress granules and the surprising possibility that stress-induced gene mRNAs could behave fundamentally differently than constitutively expressed mRNAs. Third, upon dsRNA stress, G3BP1/2-deficient cells have increased interferon responses and apoptotic signaling, suggesting a potential role for key stress granule proteins in regulating innate immune factors or stress-induced gene expression (Paget et al. 2023). Concordantly, depletion of a G3BP2 isoform altered the expression of cell survival genes during stress, suggesting a role for G3BP proteins in gene expression reprogramming (Liboy-Lugo et al. 2024). Together, these findings suggest new and alternative roles of stress granule function in mediating the ISR that must be further investigated.

The conflicting evidence on the relationship between stress-induced gene mRNAs and stress granules prompted us to test the hypothesis that association of stress-induced gene mRNAs with ribosomes inhibits their assembly into stress granules. We used chemical genetics, polysome profiling, and imaging of single endogenous and reporter mRNAs to evaluate the role of translation status and ribosome association in regulating stress-induced gene mRNA localization to stress granules in human cells. We provide evidence that stress-induced gene mRNAs that harbor uORFs including *ATF4* and *GADD34*, but not other candidate stress-induced genes, are translated during arsenite stress, and a fraction of these mRNAs localize to stress granules. We demonstrate that including uORF sequences that promote translation during stress in reporter mRNAs reduces mRNA localization to stress granules in a ribosome-dependent manner. Furthermore, we found that immobilization of one or more ribosomes on mRNAs is sufficient to block stress granule assembly and inhibit stress-induced gene mRNA localization to stress granules. These data suggest that ribosome association with uORFs inhibits stress-induced gene mRNA localization to stress granules and support the model that stress granules are sites of translation suppression.

Results

ATF4 *and* GADD34 *are translationally induced upon arsenite stress*

To determine whether candidate stress-induced gene mRNAs are translated during arsenite stress and directly

assess ribosome association with these mRNAs under conditions commonly used to study stress granules, we performed polysome profiling and RT-qPCR. We collected polysome fractions to detect mRNAs sedimenting with free RNPs (RNP peak, 40S, and 60S), monosomes/light polysomes (one to two ribosomes), or heavy polysomes (three or more ribosomes) in unstressed and stressed cells. We examined the constitutively expressed gene *GAPDH* and the candidate stress-induced genes *ATF4*, *GADD34*, *HSPA1A*, *HSPA1B*, *JUN*, and *EPRS1* (Young and Wek 2016). We chose stress-induced gene candidates that vary in length, molecular functions, and *cis*-regulatory elements. *ATF4* (1419 nt) and *GADD34* (2350 nt) contain well-characterized uORFs, and their translational upregulation during the stress response has been studied extensively (Novoa et al. 2001; Vattem and Wek 2004; Andreev et al. 2015). *JUN* (3257 nt) encodes a transcription factor that is transcriptionally induced upon arsenite stress (Andreev et al. 2015), *EPRS1* (4862 nt) encodes an ATF4-induced glutamyl-prolyl tRNA synthetase (Han et al. 2013; Neill and Masson 2023), and *HSPA1A* (2400 nt) and *HSPA1B* (2517 nt) encode HSP70 chaperones that are upregulated upon heat and arsenite stress. Robust polysomes were detected in unstressed conditions with a polysome:monosome ratio of 8.6 ± 0.3 (Fig. 1A). Arsenite stress caused polysome collapse and the accumulation of inactive or vacant 80S ribosomes (Fig. 1A) with a polysome: monosome ratio of 0.3 ± 0.1, which is consistent with past work (Kedersha et al. 2000; Dang et al. 2006; Andreev et al. 2015; Liu and Qian 2016; Guo et al. 2024). We demonstrated that the constitutively expressed *GAPDH* mRNA was translationally repressed during stress, as these mRNAs shifted from heavy polysomes in unstressed cells to free RNPs and monosomes/light polysomes upon arsenite stress (Fig. 1B,C; Supplemental Fig. S1A).

A key observation was that *ATF4* and *GADD34* mRNAs, but not other candidate stress-induced gene mRNAs, were translationally upregulated upon arsenite stress. The majority of *ATF4* and *GADD34* mRNAs sedimented with free RNPs and monosomes/light polysomes in unstressed cells (78.9% and 60.6%, respectively), and these mRNAs shifted to heavy polysomes after arsenite stress (61.3% and 53.1%, respectively), indicating that they are translationally upregulated during stress (Fig. 1B,C; Supplemental Fig. S1A). We observed that all other stress-induced mRNAs tested were translationally repressed during arsenite stress, as they shifted from heavy polysomes in unstressed conditions to free RNPs and light polysomes during stress (Fig. 1B,C; Supplemental Fig. S1A). The analysis of published ribo-seq data sets (Andreev et al. 2015) showed increased footprints on *ATF4* and *GADD34*, but not other stress-induced or constitutively expressed gene mRNAs, in ribosome-protected fragments upon 40 µM arsenite stress (Supplemental Fig. S1B). Western blotting and RT-qPCR showed that protein and RNA levels did not always predict whether mRNAs were associated with heavy polysomes during stress (Supplemental Fig. S2), likely due to differences in protein and RNA stability, reinforcing the need to directly measure mRNA association with ribosomes to establish translation activity. These results demonstrate that *ATF4* and *GADD34*, but not other candidate stress-induced genes, are translationally induced upon arsenite stress.

Steady-state localization of candidate stress-induced gene mRNAs to stress granules

To determine whether stress-induced gene mRNAs localize to stress granules, we applied single-molecule fluorescence in situ hybridization (smFISH) and quantified the percentage of endogenous stress-induced gene mRNA localized to stress granules marked by GFP-G3BP1 (Burke et al. 2020) in arsenite-stressed U-2 OS cells. We performed local normalization filtering on the GFP channel of images to accurately segment stress granules and mRNA spots using a modified version of FISH-Quant and to provide an unbiased and consistent analysis pipeline across all samples (Supplemental Fig. S3A; Imbert et al. 2022). Local normalization filtering for stress granule segmentation was critical, as GFP levels are inconsistent at the subcellular level and between cells, and the accurate segmentation of stress granules was verified by eye in each image prior to quantification. We demonstrated that the results from this image analysis pipeline showed strong positive correlation in the percentage of mRNAs localized to stress granules with images quantified by hand (Supplemental Fig. S3B), and the percentage of localization of constitutive mRNAs *GAPDH*, *NORAD*, and *AHNAK* to stress granules agreed with previous studies (Fig. 2; Khong et al. 2017; Moon et al. 2020).

We observed that ~25% of *ATF4* and *GADD34* mRNAs localized to stress granules, consistent with the idea that the majority of these transcripts are being translated and excluded from stress granules, as <50% of these transcripts colocalize with stress granules (Fig. 2B). However, <50% of the translationally repressed *HSPA1A* (26.5% ± 1.1%), *HSPA1B* (26.5% ± 1.0%), *JUN* (40.1% ± 1.5%), and *GAPDH* (15.7% ± 0.75%) mRNAs localize to stress granules after 45 min of arsenite stress (Fig. 2C,D). These results suggest translation status, while important, is not the only factor contributing to stress granule localization, in agreement with other studies demonstrating that RNA length is correlated with stress granule enrichment (Khong et al. 2017; Namkoong et al. 2018; Padrón et al. 2019; van Leeuwen et al. 2022; Curdy et al. 2023; Ren et al. 2023). Indeed, although other factors are correlated with mRNA localization to stress granules in some cases (e.g., mRNA modifications and RNA binding protein sites), we observed a positive correlation between the candidate stress-induced gene mRNA lengths and the percentage of colocalization in stress granules (Supplemental Fig. S3C). Intriguingly, ~72% of *EPRS1* mRNAs were enriched in stress granules to an extent similar to that of *AHNAK* and *NORAD* (Fig. 2C,D). Finally, we observed that the duration of stress did not impact the localization of any RNAs to stress granules with the exception of *JUN*, which displays a 5.4% increase in stress granule localization from 45 to 90 min after stress (Fig. 2C). Therefore, stress-induced genes as a class are variably enriched in stress granules.

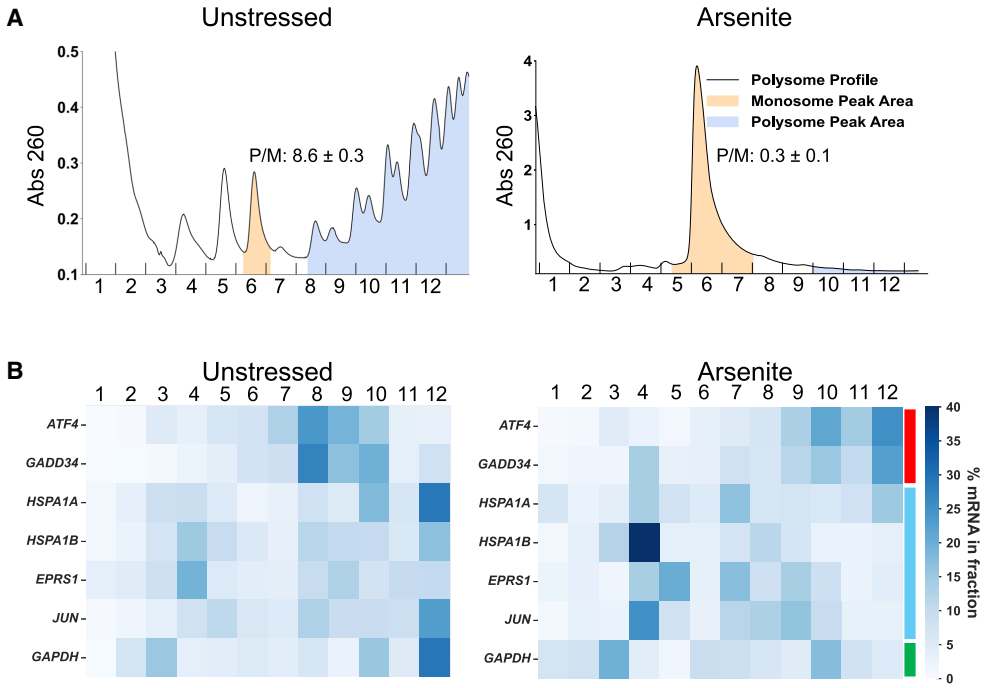

C

	Unstressed Free	Unstressed Light	Unstressed Heavy	Arsenite Free	Arsenite Light	Arsenite Heavy
ATF4:	15.6% ± 1.4%	63.3% ± 4.6%	21.1% ± 4.0%	9.8% ± 2.5%	28.9%* ± 5.7%	61.3%* ± 3.5%
GADD34:	8.2% ± 1.2%	52.4% ± 5.0%	39.4% ± 3.8%	12.9% ± 3.7%	33.9%* ± 5.0%	53.1%* ± 1.3%
HSPA1A:	27.9% ± 15.3%	18.8% ± 9.4%	53.3% ± 21.5%	34.8% ± 9.9%	35.6% ± 19.9%	29.3%* ± 17.2%
HSPA1B:	41.5% ± 5.0%	26.5% ± 5.9%	32.0% ± 0.92%	57.8% ± 2.1%	31.2% ± 0.92%	11.0%*** ± 3.0%
EPRS1:	41.5% ± 12.7%	31.0% ± 11.4%	27.5% ± 1.3%	41.6% ± 5.4%	42.9% ± 0.5%	15.5%* ± 5.3%
JUN:	25.5% ± 4.9%	33.4% ± 4.3%	41.1% ± 0.8%	39.9% ± 11.1%	44.1% ± 9.9%	16.0%*** ± 1.5%
GAPDH:	31.3% ± 11.6%	18.8% ± 8.7%	49.9% ± 16.3%	40.7% ± 7.5%	29.0% ± 11.8%	30.2% ± 7.8%

Figure 1. Stress-induced genes *ATF4* and *GADD34* are translationally upregulated during arsenite stress. (*A*) Representative polysome profiles of U-2 OS cells unstressed or stressed with 250 µM arsenite for 45 min, with orange shading representing the monosome peak and light blue representing polysomes. P/M is the polysome:monosome ratio of three independent experiments ±SEM Collected fractions are indicated *below* each profile. (*B*) Total RNA was isolated from the fractions shown in *A*, and RT-qPCR was performed. Heat maps display the average percentage of mRNA from RT-qPCR analysis in each polysome fraction corresponding to polysome profiles from unstressed and stressed cells ($n = 3$). Color coding represents stress-induced gene mRNAs that are translationally induced upon arsenite treatment (red), stress-induced gene mRNAs that are translationally repressed upon arsenite treatment (blue), or constitutive mRNAs that are translationally repressed upon arsenite treatment (green). (*C*) The average percentage of mRNA sedimenting with free (fractions 1–5), light (fractions 6–9), and heavy (fractions 10–12) polysomes ±SEM, corresponding to polysome profiles from unstressed and stressed cells ($n = 3$), is shown. Color coding is as in *B*. One-way ANOVA tests were done to determine the significance between unstressed and stressed conditions. (*) $P < 0.05$ and (***) $P < 0.005$. See also Supplemental Figures S1 and S2.

A single initiating ribosome is sufficient to block stress granule assembly

We reasoned that if stress granules can support translation of stress-induced genes, then trapping mRNAs within a single initiating ribosome would have no effect on stress granule assembly. Thus, we treated cells with harringtonine to trap initiating ribosomes at the start codon on mRNAs by inhibiting the first step of elongation (Huang 1975; Fresno et al. 1977; Ingolia et al. 2012). Polysome profiling confirmed that harringtonine treatment for 10 or 30 min leads to rapid ribosome runoff and accumulation of 80S complexes, as expected (Fig. 3A,B).

Notably, pretreatment of cells with harringtonine to trap mRNAs within a single initiating ribosome blocked stress granule assembly upon arsenite stress (Fig. 3C–E;

Supplemental Movie S1), as suggested by a recent study (Fedorovskiy et al. 2023). Although cells treated with arsenite formed stress granules marked by GFP-G3BP1 beginning at 30 min, stress granule assembly was not observed in arsenite-stressed cells pretreated with harringtonine up to 60 min later (the duration of imaging) (Fig. 3D,E; Supplemental Movie S1). Fixation of cells immediately after live-cell imaging followed by immunofluorescence microscopy with fluorescence in situ hybridization to detect the stress granule protein UBAP2L and polyadenylated RNAs confirmed that harringtonine pretreatment blocked stress granule assembly during arsenite stress (Fig. 3F). Harringtonine-treated fixed cells often had few (<1% of cytoplasmic area), small (<500 nm in diameter), low-intensity UBAP2L and GFP-G3BP1 foci that were not observed in live cells, a discrepancy likely arising from fixation (Supplemental Fig. S4; Irgen-Gioro et al. 2022). Live-cell imaging of cells expressing the stress

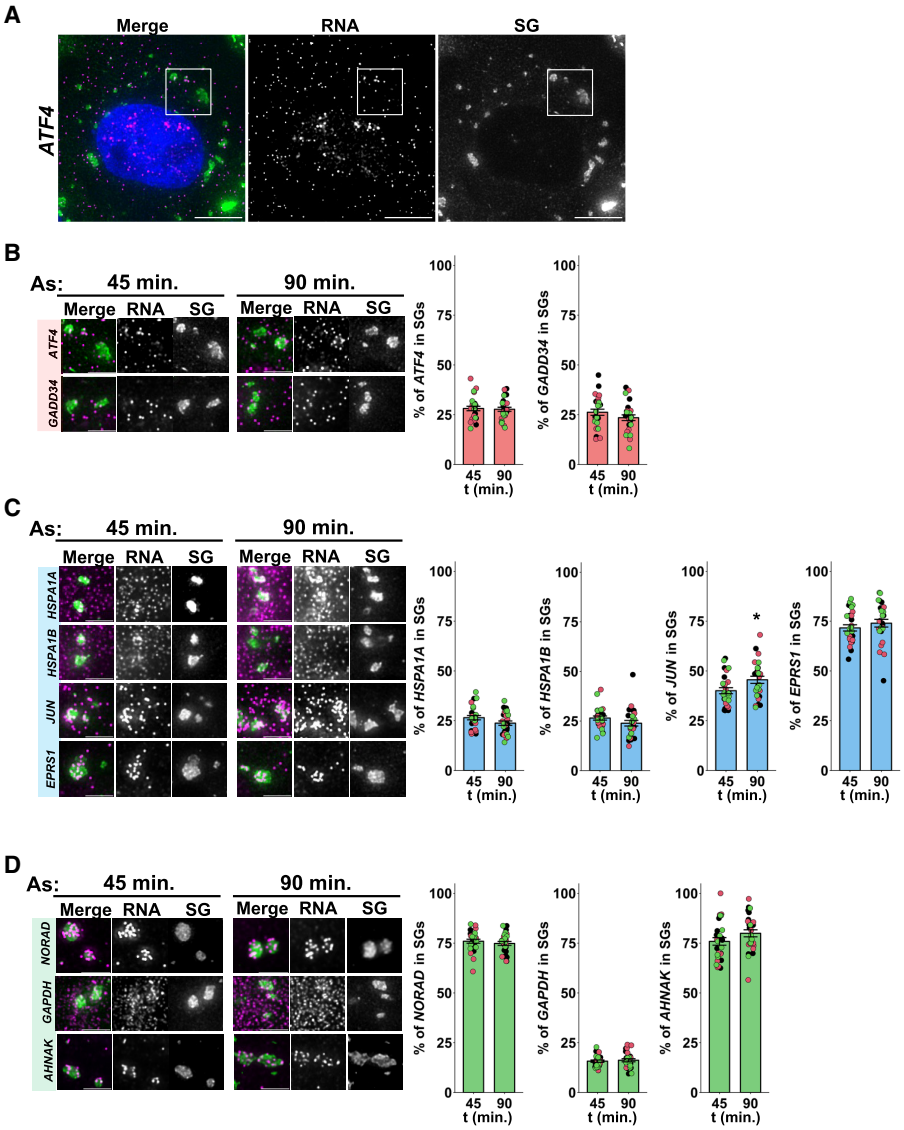

Figure 2. Steady-state localization of candidate stress-induced gene mRNAs to stress granules. (*A–D*) Stressed (250 µM arsenite for 45 or 90 min) U-2 OS cells stably expressing GFP-G3BP1 were fixed, and smFISH was performed for RNAs encoding stress-induced genes that are translationally upregulated (*A*,*B*; red), stress-induced genes that are translationally downregulated (*C*; blue), or constitutively expressed genes (*D*; green). (*A*) Representative images are shown of an entire cell (45 min arsenite stress). Stress granules (SGs) are shown in green, *ATF4* RNA is shown in magenta, and nuclei are shown in blue. Scale bar, 10 µm. (*B–D*, *left*) Representative zoomed-in images ($n = 3$) of cells stressed with 250 µM arsenite (As) for 45 or 90 min. Images were taken at 100× magnification, with the GFP-G3BP1 stress granule (SG) marker shown in green and RNA shown in magenta. Scale bars, 5 µm. (*Right*) The average ± SEM of the percentage of cytoplasmic RNA localized to stress granules per cell ($n = 27$ cells) from three independent experiments (denoted as green, red, and black circles, with individual circles representing a single cell) is shown. One-way ANOVA tests were done to determine the significance between 45 and 90 min arsenite conditions. (*) $P < 0.05$. See also Supplemental Figure S3.

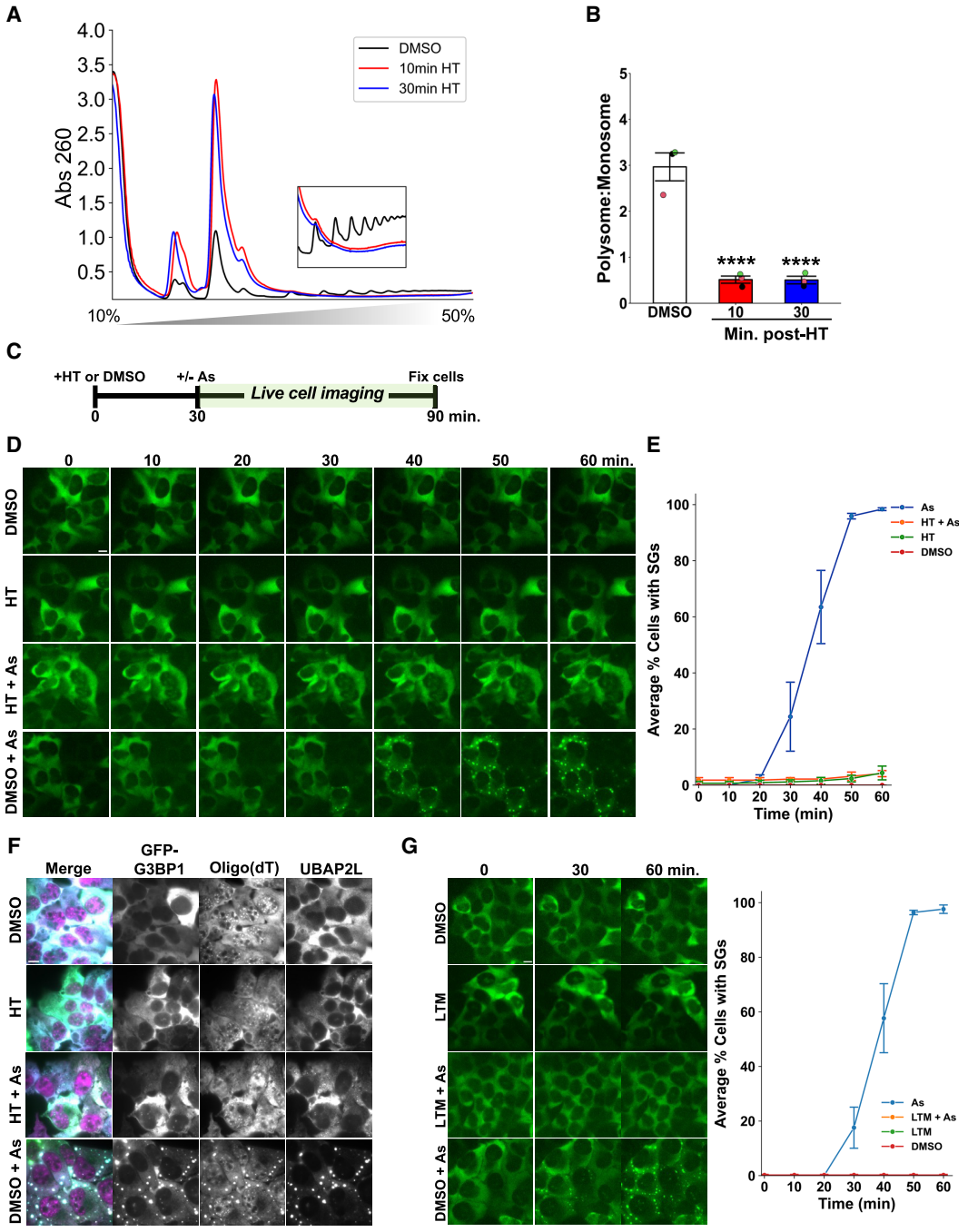

Figure 3. A single initiating ribosome blocks stress granule assembly. (*A*) Representative polysome profiles ($n = 3$) of U-2 OS cells treated with 0.1% DMSO (carrier; black) or 2 µg/mL harringtonine (HT) for 10 min (red) or 30 min (blue) followed by cycloheximide addition. The *X*-axis represents the distance down the sucrose gradient from 10% to 50%. (*B*) Average ± SEM is reported for the polysome to monosome ratio from polysome profiles in *A* from $n = 3$ replicates (denoted as green, red, and black circles). ANOVA tests were done to determine the significance between the DMSO and HT-treated conditions. (****) $P < 0.001$. (*C*) Schematic of experimental time line for *D*–*F* (2 µg/mL harringtonine [HT] and 250 µMarsenite [As]). (*D*) U-2 OS cells were pretreated with DMSO or harringtonine for 30 min followed by live-cell imaging at 40× magnification with or without arsenite for 60 min. Images were taken every minute, and representative images ($n = 3$ for all times and conditions except the DMSO 20 min time point, which is $n = 2$) of U-2 OS cells stably expressing GFP-G3BP1 (green) are shown. Scale bar, 10 µm. See also Supplemental Move S1. (*E*) The average ± SEM of the percentage of cells in a frame positive for stress granules corresponding to images in *D* is shown. (*F*) After live-cell imaging (shown in *D*,*E*), cells were fixed and stained for polyadenylated RNA [oligo(dT); magenta] and stress granule protein UBAP2L (cyan). GFP-G3BP1 is shown in green ($n = 2$). Scale bar, 5 µm. See also Supplemental Figure S4. (*G*) U-2 OS cells were pretreated with DMSO or 50 µM lactimidomycin (LTM) for 30 min followed by live-cell imaging with or without arsenite as done in *D*. (*Left*) Representative images. Scale bar, 10 µm. (*Right*) The average ± SEM of the percentage of cells in a frame with stress granules ($n = 3$) is shown. See also Supplemental Movies S2–S4 and Supplemental Figure S5.

granule marker protein mRuby2-PABPC1 (Burke et al. 2020) confirmed that stress granule assembly is inhibited in the presence of harringtonine (Supplemental Fig. S5A; Supplemental Movie S2). Cotreatment of cells with arsenite and harringtonine or the elongation inhibitor emetine, which traps mRNAs within polysomes, also significantly reduced stress granule assembly in fixed cells (Supplemental Fig. S6B), in line with previous work (Kedersha et al. 2000). The natural product lactimidomycin also traps mRNAs within initiating ribosomes (Schneider-Poetsch et al. 2010; Lee et al. 2012), and we observed that lactimidomycin also inhibited stress granule assembly in the presence of arsenite (Fig. 3G; Supplemental Movie S3). Thus, trapping mRNAs within initiating monosomes inhibits stress granule assembly.

Previous work has suggested that inhibiting translation initiation (e.g., with harringtonine or lactimidomycin) can induce 40S ribosomal subunit ubiquitination and subsequent degradation through the initiation of a ribosome-associated quality control pathway (Garshott et al. 2021). To rule out the possibility that 40S protein ubiquitylation and the associated degradation were responsible for blocking stress granule formation, we treated cells with harringtonine and assessed stress granule assembly after harringtonine washout and upon addition of arsenite. We observed that stress granules assemble within 1 h after harringtonine washout (Supplemental Fig. S5B; Supplemental Movie S4). Given that these experiments were performed under conditions of limited translation when cells would be unable to translate new 40S subunits, these results suggest that the inhibition of stress granule assembly upon harringtonine treatment is not due to 40S subunit degradation. Therefore, the association of a single ribosome with an mRNA changes its conformation and/or interaction partners in a way that prohibits stress granule formation beyond the blocking or remodeling of the open reading frame by elongating ribosomes.

Ribosome association limits stress-induced gene mRNA accumulation in stress granules

We next took a chemical genetics approach to test the hypothesis that ribosome association inhibits partitioning of *ATF4* and *GADD34* into stress granules. We selected a set of translation modulators that (1) prevent ribosome association with mRNAs by blocking initiation, (2) release mRNAs from elongating ribosomes, (3) trap an initiating 80S ribosome on mRNAs, or (4) trap elongating ribosomes on mRNAs (Supplemental Fig. S6A). Prior work demonstrated that releasing constitutively expressed mRNAs from ribosomes with puromycin increases their localization to stress granules (Khong and Parker 2018; Moon et al. 2020) and can cause stress granule assembly (Kedersha et al. 2000; Markmiller et al. 2018). Conversely, trapping mRNAs on ribosomes with cycloheximide or emetine reduces constitutively expressed mRNA localization to stress granules (Khong and Parker 2018) and blocks stress granule assembly (Kedersha et al. 2000). To limit the impacts of translation modulators on stress granule properties that occur when inhibitors are added simultaneously with the stress (Supplemental Fig. S6B), we stressed cells for 35 min with arsenite to allow stress granule assembly and then added translation inhibitors for the last 10 min prior to fixation. We confirmed that none of these treatments altered stress granule size (Supplemental Fig. S6C). We performed smFISH to detect the translationally upregulated stress-induced genes that we had established as translating using polysome profiling and RT-qPCR. Controls included translationally repressed stress-induced genes, constitutively expressed mRNAs, and the noncoding RNA *NORAD*.

We found that inhibiting translation initiation or releasing mRNAs from ribosomes significantly increased the recruitment of *ATF4* and *GADD34* mRNAs to stress granules. Treatment of cells with the cap-dependent translation initiation inhibitor rocaglamide A (which stabilizes eIF4A on the 5′ UTRs of mRNAs, blocks 43S scanning, and prevents ribosome association) (Iwasaki et al. 2016, 2019) significantly increased the accumulation of *ATF4* and *GADD34* in stress granules by 21% and 47% (respectively) relative to the DMSO control (Fig. 4A). Concordantly, release of translating ribosomes from mRNAs with the tyrosyl-tRNA mimic puromycin (Nathans 1964; Enam et al. 2020; Hobson et al. 2020) similarly increased the relative amount of *ATF4* and *GADD34* mRNA localized to stress granules by 17% and 30%, respectively (Fig. 4A). Rocaglamide A and puromycin caused a similar increase in the localization of *ATF4* and *GADD34* to stress granules induced by DTT stress, demonstrating that these results are not stress-specific (Supplemental Fig. S7). A further relative increase in *ATF4* and *GADD34* localization to stress granules (by 38% and 58%, respectively) was observed in cells cotreated with rocaglamide A and puromycin, as would be expected upon forced ribosome release and blocked reinitiation (Fig. 4A). The observed increase in *ATF4* and *GADD34* localization to stress granules upon cotreatment with rocaglamide A and puromycin suggests that these transcripts continuously reinitiate translation during arsenite stress. Localization of other candidate stress-induced or constitutively expressed mRNAs, or the noncoding RNA *NORAD*, to stress granules was unaffected by rocaglamide A and/or puromycin treatment (Fig. 4B,C), indicating that the increased recruitment of *ATF4* and *GADD34* to stress granules was due to changes in translation and not impacts on stress granule properties. Together, these results suggest that *ATF4* and *GADD34* are translated through cap-dependent mechanisms and that association with ribosomes inhibits RNA localization to stress granules.

We next established that increasing ribosome occupancy on stress-induced gene mRNAs reduced their localization to stress granules. Treating cells with harringtonine to trap initiating ribosomes at the start codon (Huang 1975; Fresno et al. 1977; Ingolia et al. 2012) or with emetine, which binds the E site of the 40S ribosomal subunit and immobilizes elongating ribosomes on mRNAs (Grollman 1968; Gupta and Siminovitch 1977; Wong et al. 2014), significantly reduced the percentage of *ATF4* and *GADD34* that localized to stress granules (Fig. 5A). We

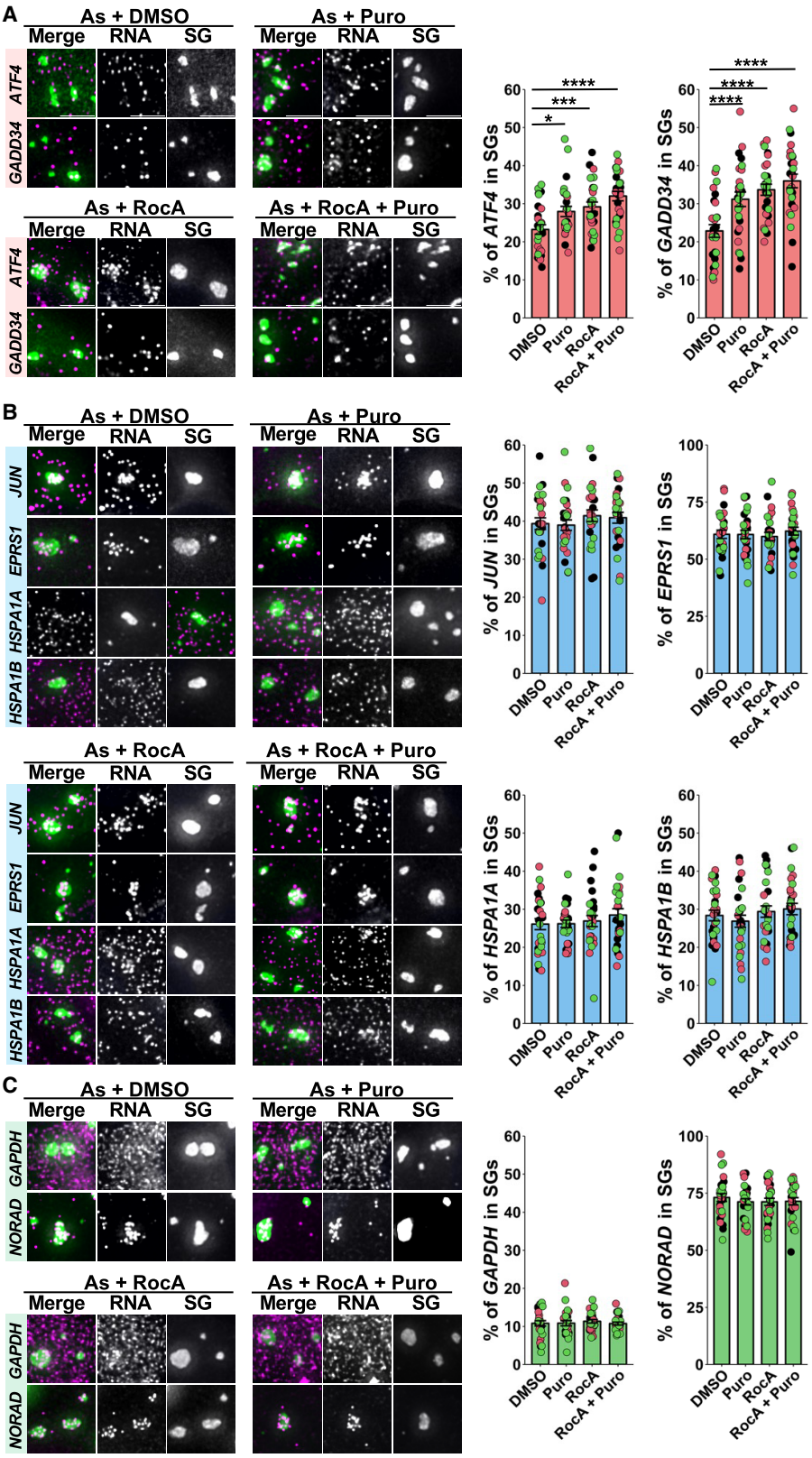

Figure 4. Ribosome release or inhibition of ribosome association with *ATF4* or *GADD34* increases their partitioning into stress granules. (*A–C*) U-2 OS cells stably expressing GFP-G3BP1 were stressed with 250 µM arsenite (As) for 35 min followed by addition of 0.1% DMSO, 1 µM rocaglamide A (RocA), 2 µg/mL puromycin (Puro), or rocaglamide A and puromycin for 10 min. smFISH was performed on fixed cells to determine the localization of RNAs encoding stress-induced genes that are translationally upregulated (*A*, red), stress-induced genes that are translationally downregulated (*B*; blue), or constitutively expressed genes (*C*; green). (*Left*) Representative images are shown with RNA in magenta and stress granules (SGs) in green, as labeled with GFP-G3BP1. Scale bar, 5 µm. (*Right*) The average ± SEM of the percentage of cytoplasmic RNA localized to stress granules per cell ($n = 27$ cells) from three independent replicates (denoted as green, red, and black circles, with individual circles representing a single cell) is shown. One-way ANOVA tests were done to determine significance between the DMSO condition and other treatments. (*) $P < 0.05$, (***) $P < 0.005$, (****) $P < 0.001$. See also Supplemental Figures S3, S6, and S7.

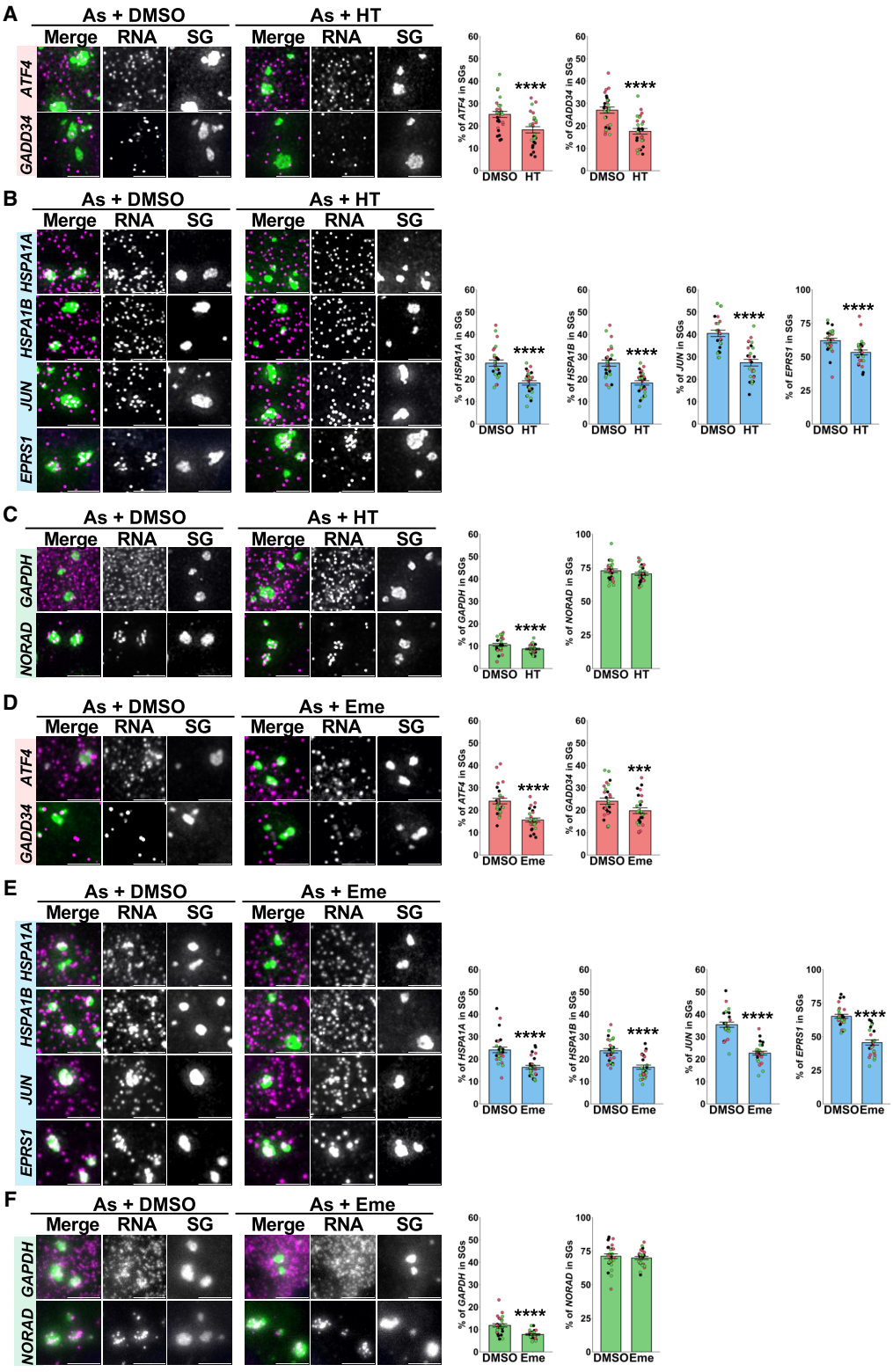

Figure 5. Stabilizing one or more ribosomes on mRNAs reduces their localization to stress granules. (*A–F*) U-2 OS cells stably expressing GFP-G3BP1 were stressed with 250 µM arsenite (As) for 35 min followed by addition of 0.1% DMSO, 2 µg/mL harringtonine (HT), or 45 µM emetine (Eme) for 10 min. smFISH was performed on fixed cells to determine the localization of RNAs encoding stress-induced genes that are translationally upregulated (*A*,*D*; red), stress-induced genes that are translationally downregulated (*B*,*E*; blue), or constitutively expressed genes (*C*,*F*; green). (*Left*) Representative images are shown with RNA in magenta and stress granules (SGs) in green (GFP-G3BP1). Scale bar, 5 µm. (*Right*) The average ± SEM of the percentage of cytoplasmic RNA localized to stress granules per cell ($n = 27$ cells) from three independent replicates (denoted as green, red, and black circles, with individual circles representing a single cell) is shown. One-way ANOVA tests were done to determine the significance between DMSO condition and other treatments. (****) $P < 0.001$. See also Supplemental Figures S3, S6, and S7.

also observed that the localization of translationally repressed stress-induced or constitutively expressed mRNAs to stress granules was reduced with emetine or harringtonine treatment (Fig. 5B–F), suggesting that ribosomes are continuing to run off transcripts 35 min after arsenite stress. A prior study also observed that recruitment of constitutively expressed *AHNAK* to stress granules is limited by the translation elongation inhibitor cycloheximide during arsenite stress (Khong and Parker 2018). Similar results were observed in cells treated with DTT stress (Supplemental Fig. S7), as the fraction of *ATF4*, *GADD34*, and, to a lesser extent, *GAPDH* mRNA localized to DTT-induced stress granules was significantly decreased in harringtonine- and emetine-treated cells compared with the DMSO control. There was no change in *NORAD* accumulation in arsenite-induced stress granules in either harringtonine or emetine treatments, indicating that general stress granule properties were not altered and that our observations were likely due to changes in translation (Fig. 5C,F). However, cells stressed with DTT and treated with harringtonine displayed a small decrease in *NORAD* localization to stress granules (Supplemental Fig. S7), suggesting that DTT-induced stress granules are more sensitive to translation inhibitors that increase ribosome occupancy on mRNAs than arsenite-induced stress granules. Together, these results demonstrate that association with one or more ribosomes is sufficient to reduce mRNA localization to stress granules.

uORFs inhibit mRNA localization to stress granules through ribosome association

We next evaluated whether uORFs alone are sufficient to inhibit mRNA localization to stress granules using two approaches. First, we assessed the impact of translation initiation and elongation inhibitors on the localization of two additional uORF-containing stress-induced genes: *IFRD1* (Zhao et al. 2010) and *UCP2* (Hurtaud et al. 2006). Ribosome footprinting results (Andreev et al. 2015) suggest that these two mRNAs harbor uORFs that promote their translation during arsenite stress. We observed that both *IFRD1* and *UCP2* exhibited significantly increased localization to stress granules in the presence of rocaglamide A (by 58% and 53%, respectively) and puromycin (by 65% and 49%, respectively), whereas harringtonine and emetine reduced their localization to stress granules (Fig. 6A). We examined the localization of two additional constitutively expressed gene mRNAs, *ACTB* and *AHNAK*, to stress granules in the same cells in which we examined *IFRD1* and *UCP2* using smFISH probes labeled with two different fluors. We observed that the localization of *ACTB* and *AHNAK* did not change upon rocaglamide A or puromycin treatment (Fig. 6A). As previously observed with *GAPDH*, harringtonine and emetine reduced the localization of both *ACTB* and *AHNAK* to stress granules (Fig. 6A). We compared the average percentage change in mRNA localization to stress granules upon translation inhibitor treatments across all endogenous genes examined and observed that only mRNAs containing uORFs had increased localization to stress granules with rocaglamide A or puromycin treatment (Fig. 6B). Together, these results suggest that the association of ribosomes with uORFs on translating stress-induced genes during stress inhibits their localization to stress granules.

To directly test the hypothesis that uORFs inhibit the localization of mRNAs to stress granules, we made reporter mRNA constructs harboring the 5′ untranslated regions containing the uORFs from *ATF4* or *GADD34* upstream of a main open reading frame encoding luciferase. We then created mutant reporter mRNAs in which the three AUG start codons (Met) of the *ATF4* uORFs and the start codons of the two *GADD34* uORFs were changed to GCC (Ala) to abrogate uORF function and control for mRNA length (Fig. 7A). We placed these reporters under the control of dox-inducible promoters and stably integrated them in U-2 OS cells expressing GFP-G3BP1. After dox induction, cells were stressed with arsenite for 45 min and pulsed with translation inhibitors 10 min prior to fixation. smFISH was done using probes complementary to the luciferase open reading frame, and analysis was done as described above for endogenous mRNA localization.

A key observation is that the reporters harboring either wild-type *ATF4* or *GADD34* uORFs were localized to stress granules significantly less (by ∼30%) than mutant *ATF4* or *GADD34* uORF transcripts (Fig. 7B,C). These results suggest that uORFs inhibit mRNA localization to stress granules. We next tested whether releasing ribosomes, preventing ribosome association with mRNAs, or trapping ribosomes on mRNAs would increase or decrease (respectively) the localization of uORF-containing reporters to stress granules. Importantly, we observed that rocaglamide A and puromycin increased the localization of wild-type, but not mutant, *ATF4* and *GADD34* uORF-containing reporters to stress granules (Fig. 7B,C). Compared with DMSO-treated cells, the *ATF4* uORF-containing reporter increased localization to stress granules by 40% with rocaglamide A and 37% with puromycin, whereas the *GADD34* uORF-containing reporter increased localization to stress granules by 31% in both conditions (Fig. 7B,C). Treatment with the translation elongation inhibitors harringtonine and emetine reduced the localization of wild-type and mutant *ATF4* and *GADD34* uORF-containing reporters (Fig. 7B,C). Taken together, these results indicate that uORFs limit mRNA localization to stress granules in a manner dependent on ribosome association.

Discussion

We provide evidence that ribosome association inhibits stress-induced gene mRNA assembly into stress granules and suggest that uORFs play a key role in limiting mRNA condensation. We found that the translationally upregulated genes *ATF4*, *GADD34*, and other uORF-containing stress-induced gene mRNAs displayed increased partitioning to stress granules upon the prevention of translation initiation or their release from polysomes. We observed that assembly of all mRNAs into stress granules

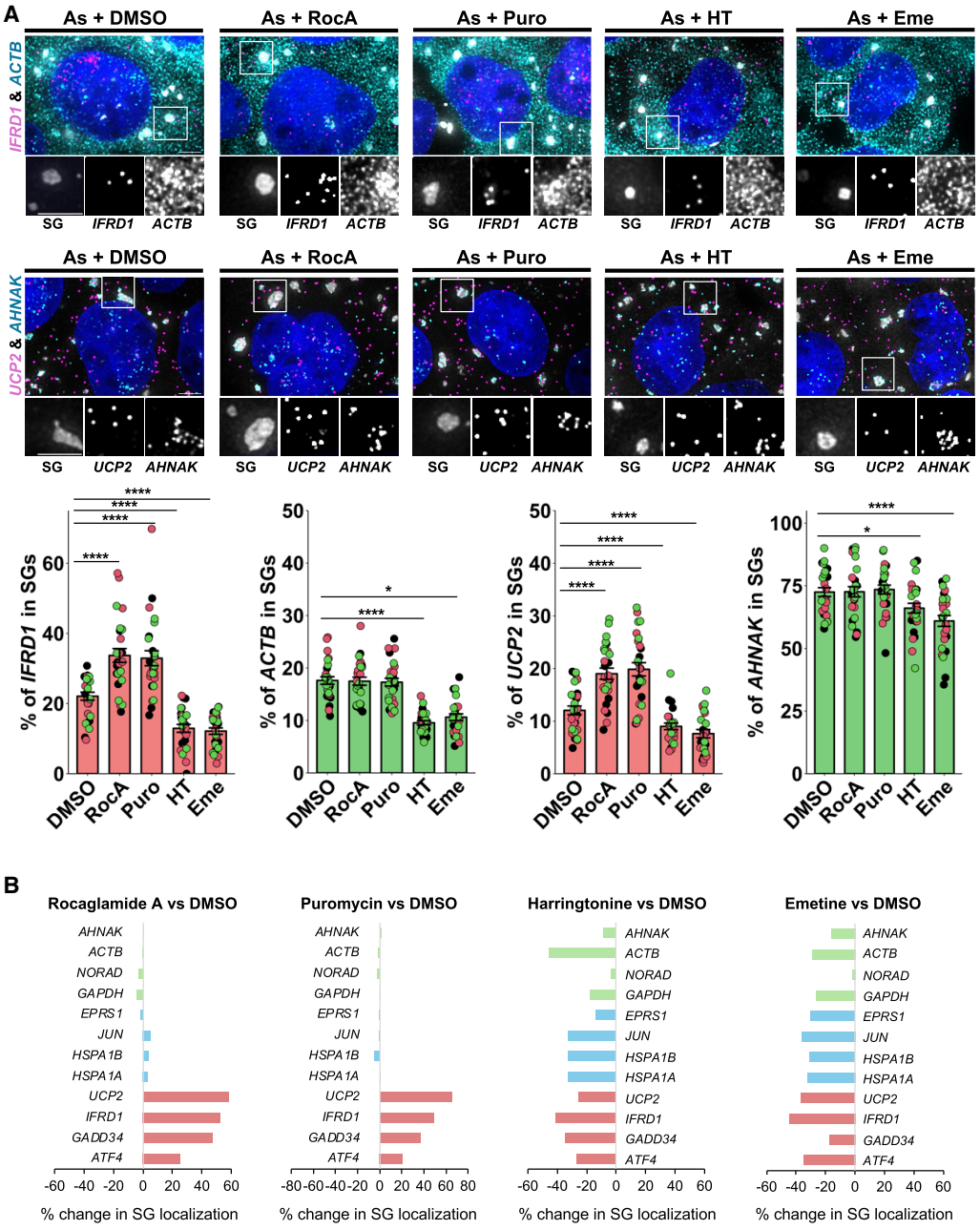

Figure 6. Ribosome association inhibits localization of endogenous mRNAs with uORFs to stress granules. (*A*) U-2 OS cells stably expressing GFP-G3BP1 were stressed with 250 µM arsenite for 35 min followed by addition of 0.1% DMSO, 1 µM rocaglamide A (RocA), 2 µg/mL puromycin (Puro), 2 µg/mL harringtonine (HT), or 45 µM emetine. smFISH was performed on fixed cells to determine the localization of RNAs encoding stress-induced genes with uORFs (*IFRD1* and *UCP2*) or constitutively expressed genes (*ACTB* and *AHNAK*). (*Top*) Representative images are shown with stress-induced gene mRNA in magenta, constitutively expressed mRNAs in cyan, nuclei in blue, and stress granules (SGs) in gray as labeled with GFP-G3BP1, with zoomed-in images *below* the full cell images. Scale bars, 5 µm. (*Bottom*) The average ± SEM of the percentage of cytoplasmic RNA localized to stress granules per cell ($n = 27$) from three independent replicates (denoted as green, red, and black circles, with individual circles representing a single cell) is shown. One-way ANOVA tests were done to determine the significance between the DMSO condition and other treatments. (*) $P < 0.05$, (****) $P < 0.001$. (*B*) Summary of the average percentage change of stress granule localization for every endogenous mRNA tested under the different inhibitor treatments compared with the control DMSO treatment ($n = 3$). Green bars represent constitutively expressed mRNAs, blue represents stress-induced gene mRNAs that are translationally downregulated, and red represents uORF-containing stress-induced gene mRNAs. See also Supplemental Figures S3 and S6.

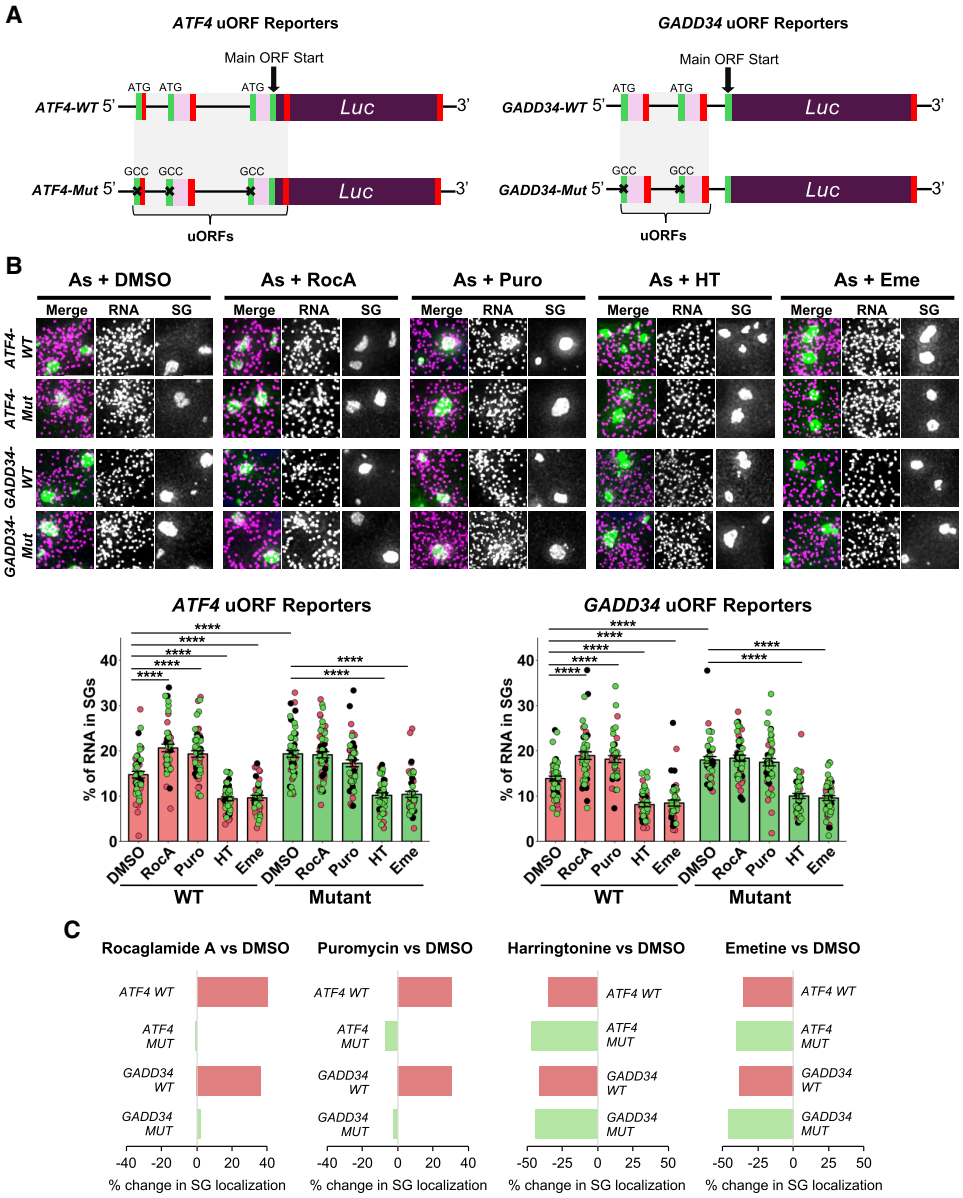

Figure 7. Ribosome association inhibits localization of reporter mRNAs containing *ATF4* or *GADD34* uORFs to stress granules. (*A*) Schematic of wild-type (WT) and mutant (Mut) *ATF4* and *GADD34* uORF reporter constructs. Green represents start codons, red represents stop codons, pink represents uORF sequences, and purple represents the main human-optimized *Renilla* luciferase (Luc) ORF. All 5′ UTR (uORF) start codons were mutated from ATG (Met) to GCC (Ala) in the Mut-ORF constructs to ablate uORFs. (*B*) U-2 OS cells stably expressing the reporters described in *A* under a dox-inducible promoter and GFP-G3BP1 to mark stress granules were treated with 200 ng/mL doxycycline for 24 h and stressed with 250 µM arsenite for 35 min followed by cotreatment with 0.1% DMSO, 1 µM rocaglamide A (RocA), 2 µg/mL puromycin (Puro), 2 µg/mL harringtonine (HT), or 45 µM emetine (Eme) for 10 min. smFISH was performed on fixed cells to determine the localization of *Luc* RNAs to stress granules. (*Top*) Representative images are shown with RNA in magenta and stress granules (SGs) in green. Scale bar, 5 µm. (*Bottom*) The average ± SEM of the percentage of cytoplasmic RNA localized to stress granules per cell ($n = 41$–53 cells) from three independent replicates (denoted as green, red, and black circles, with individual circles representing a single cell) is shown. One-way ANOVA tests were done to determine the significance between the DMSO condition and other treatments. (*) $P < 0.05$, (****) $P < 0.001$. (*C*) The average percentage change in stress granule localization from $n = 3$ independent experiments is shown for the reporters and conditions described in *A* and *B*.

was inhibited by their association with one or more ribosomes. Furthermore, the observations that uORF sequences are sufficient to limit mRNA localization to stress granules in a ribosome-dependent manner indicate that ribosome recruitment inhibits mRNA condensation. Together, these findings strongly suggest that stress granules cannot serve as efficient hubs of stress-induced gene translation given the inverse relationship between

ribosome association with an mRNA and its stable association with a stress granule.

The observation that a single ribosome is sufficient to inhibit mRNAs from localizing to stress granules has major implications for our understanding of stress-induced gene expression and RNP condensation. First, this finding suggests that ribosome association on uORFs is a *cis*-regulatory mechanism to prevent condensation of stress-induced gene mRNAs. Ribosomes associate with uORFs in the 5′ UTRs of stress-induced gene mRNAs such as *ATF4* and *GADD34* (Andreev et al. 2015; Smirnova et al. 2024) but are not present in other stress-induced genes (e.g., *HSPA1A/B*). In unstressed conditions, uORFs generally repress translation of the main ORFs and negatively regulate gene expression (Vattem and Wek 2004; Lee et al. 2009; Young et al. 2015; Dever et al. 2023). Translation of uORF-containing mRNAs increases when the ternary complex is limited in part by "leaky scanning" of the 43S preinitiation complex, allowing for bypass of inhibitory uORFs and reinitiation at the main ORF (Vattem and Wek 2004; Lee et al. 2009; Young et al. 2015; Dever et al. 2023). uORFs are important gene regulatory elements, as they are estimated to occur in ∼10%–50% of all human mRNAs (Kozak 1987; Matsui et al. 2007; McGillivray et al. 2018; Chothani et al. 2022), uORFs are evolutionarily conserved (Zhang et al. 2021), and uORF disruption or generation is under strong negative selection (Whiffin et al. 2020). In addition to uORFs, ribosome profiling has revealed unanticipated small ORFs (<100 amino acids) outside of annotated coding sequences (Ingolia et al. 2011; Brar et al. 2012; Brar and Weissman 2015; Chothani et al. 2022). Small ORFs and uORFs may encourage ribosomes to associate with RNAs without generating a functional protein product to prevent RNA condensation. In the context of uORFs, increased ribosome association that prevents condensation would be predicted to increase translation, whereas other RNAs condense and are translationally repressed.

Second, our results suggest that the reduced effective valency of mRNAs resulting from ribosome occupancy across the open reading frame is not the only mechanism by which ribosomes prevent stress granule assembly. Thus, stress granule assembly may not be solely driven by the formation of a scaffold from networks of interactions between ribosome-free mRNA open reading frames (Van Treeck et al. 2018; Guzikowski et al. 2019; Putnam et al. 2023). Multivalent RNA–RNA, RNA–protein, and protein–protein interactions are critical for RNP granule assembly and/or stability (Bounedjah et al. 2014; Banani et al. 2016; Shin et al. 2017; Van Treeck et al. 2018; Moon et al. 2019; Zhang et al. 2019; Riback et al. 2020; Sanders et al. 2020; Yang et al. 2020; Matheny et al. 2021; Freibaum et al. 2024). Stress granule assembly requires RNA–protein and RNA–RNA interactions, as G3BP1 mutants incapable of binding RNA do not form higher-order G3BP assemblies, and RNases disrupt these assemblies in vitro and in vivo (Burke et al. 2019; Guillén-Boixet et al. 2020; Sanders et al. 2020; Yang et al. 2020; Decker et al. 2022). Furthermore, RNA alone forms condensates in vitro that largely recapitulate the stress granule transcriptome (Van Treeck et al. 2018), and long, single-stranded, and unfolded RNAs capable of forming intermolecular RNA–RNA interactions are required for G3BP condensate formation in vitro (Guillén-Boixet et al. 2020; Yang et al. 2020). However, the release of mRNAs from ribosomes is necessary and sufficient for stress granule formation in wild-type cells, but ribosome release is not sufficient for stress granule assembly in some conditions, such as in cells lacking G3BP1/2 (Kedersha et al. 2016). One ribosome stalled at the start codon that shields ∼28–32 nt of an mRNA (Ferguson et al. 2023) would not be predicted to have a large impact on the available interactions permitted by a free open reading frame that would drive RNA condensation. However, mRNAs may adopt a more closed conformation through intramolecular interactions when they are assembled into a translation initiation complex. Such a closed conformation would limit intermolecular interactions, reduce effective valency, and prevent RNP granule assembly. Indeed, smFISH analyses revealed that although translating mRNAs adopt a more compact conformation than would be predicted if they were fully extended, mRNAs become further compacted when they are released from ribosomes (Adivarahan et al. 2018; Khong and Parker 2018). Harringtonine, puromycin, and arsenite cause a similar degree of mRNA compaction (Adivarahan et al. 2018), suggesting that the presence of a ribosome at the start codon does not restrict mRNAs from adopting compacted conformations. In contrast to the widely held view that polysomes shield the open reading frame to prevent stress granule assembly, these results could suggest the interpretation that a single ribosome stalled at the start codon can reduce the effective valency of nontranslating mRNAs through conformational changes, which may prevent stress granule assembly.

Another possibility is that monosomes recruit factors such as helicases, segregases, or chaperones that extend beyond the ribosome-occupied start codon and prevent RNP condensation. Ribosomes interact with RNA helicases, RNA binding proteins, proteasome subunits, chaperones, and the ubiquitin-binding protein segregase VCP (Simsek et al. 2017; Sinha et al. 2020; Popper et al. 2024; Weber et al. 2024), many of which inhibit stress granule assembly and/or promote stress granule disassembly (Buchan et al. 2013; Turakhiya et al. 2018; Wang et al. 2019; Tauber et al. 2020; Yang et al. 2020; Budkina et al. 2021; Gwon et al. 2021; Tolay and Buchberger 2021; Li et al. 2022; Ripin et al. 2024). Furthermore, protein degradation factors implicated in stress granule disassembly (Buchan et al. 2013; Turakhiya et al. 2018; Wang et al. 2019; Gwon et al. 2021; Tolay and Buchberger 2021) could be recruited to ribosomes by modifications such as 40S subunit ubiquitination that occurs with harringtonine treatment (Garshott et al. 2021). In line with this possibility, proteasome subunits, VCP, and RNA helicases cosediment with monosomes from harringtonine-treated rat cortical neurons (Popper et al. 2024). Trapping mRNAs within initiating monosomes could also prevent recruitment of proteins that bind free 40S subunits such as G3BP1 (Kedersha et al. 2016) to limit stress granule

formation. Therefore, stalled 80S ribosomes may inhibit mRNP assembly into stress granules due to the recruitment or exclusion of proteins that inhibit or promote (respectively) the multivalent interactions required for RNP granule formation.

Alternatively, trapping mRNAs in monosomes could prevent stress granule assembly by reducing the amount of preinitiation complexes available to seed stress granules (Panas et al. 2016). In this case, harringtonine or lactimidomycin would cause the degradation or sequestration of 40S and other initiation factors in monosomes (Garshott et al. 2021). In support of this idea, coimmunoprecipitation experiments demonstrated that G3BP1 preferentially interacts with free 40S subunits (Kedersha et al. 2016), and RNAi-mediated depletion of 40S subunits inhibits stress granule formation (Ohn et al. 2008). Furthermore, cryo-ET results demonstrate that preinitiation complexes and 40S ribosomal subunits are enriched in stress granules (Guo et al. 2024), as suggested by immunofluorescence microscopy (Kedersha et al. 2002). Additionally, preinitiation complexes accumulated upon eIF3b depletion enhance stress granule assembly in heat-stressed baker's yeast (Glauninger et al. 2024). Harringtonine does not inhibit preinitiation complexes from forming (Fresno et al. 1977; Garshott et al. 2021), but harringtonine-stalled ribosomes are ubiquitinated, and this leads to a reduction in 40S ribosome levels consistent with their degradation (Garshott et al. 2021). However, our observation that stress granules can assemble in the presence of arsenite within 1 h after harringtonine removal suggests that 40S degradation is unlikely to explain how harringtonine inhibits stress granule assembly, as 40S subunits would need to be newly generated to permit stress granule formation. Furthermore, the ubiquitin marks on 40S proteins (uS3 and uS5) observed upon harringtonine treatment are also deposited during arsenite stress under conditions when stress granules would be present (Garshott et al. 2021). Additional experimentation to differentiate between these possibilities may clarify the detailed mechanisms of stress granule assembly.

The observation that a single ribosome inhibits mRNA localization to stress granules supports the model that stress granules are not significant sites of active translation. These results are consistent with past work showing that locking polysomes on constitutively expressed mRNAs reduces their localization to stress granules and inhibits stress granule assembly (Kedersha et al. 2000; Bounedjah et al. 2014; Khong and Parker 2018). Furthermore, the observations that translation efficiency is negatively correlated with stress granule enrichment (Khong et al. 2017; Namkoong et al. 2018; Matheny et al. 2019; Padrón et al. 2019; Ren et al. 2023) and that mRNAs encoding proteins translated during stress are not enriched in stress granules (Baron et al. 2019) suggest that stress granules are not sites of translation activity. Live-cell single-mRNA imaging studies demonstrate that mRNAs associated with nascent proteins only interact transiently with stress granules (Moon et al. 2019, 2020), an observation that could only be made with confidence using high-frequency spatially resolved imaging across the cell volume. Because stress granules are not uniformly spherical and contain regions of low and high dynamicity, referred to as core and shell regions (Jain et al. 2016), mRNAs within translation complexes may be briefly captured within the dynamic shell or tethered to the surface of the granule (Moon et al. 2019).

Several studies using orthogonal approaches have shed additional light on the relationship between stress granules and mRNA translation. A recent cryo-ET study demonstrated that only ~1.4% of the 80S ribosomes observed in stressed cells were in a conformation suggestive of active translation, and 80S ribosomes were dramatically reduced per unit area within stress granules, thus indicating that any instances of translation within stress granules must be much less frequent than in the surrounding cytoplasm (Guo et al. 2024). Additionally, tethering mRNA reporters to optogenetically induced RNP condensates reduces the levels of the encoded protein (suggestive of translational repression) (Lee et al. 2024), and optogenetically induced stress granules require mRNAs to be released from the translating pool to form (Zhang et al. 2019). Finally, other RNP granules also harbor translationally repressed mRNAs. Embryonic P granules in *Caenorhabditis elegans* are enriched in mRNAs with low ribosome occupancy, mRNAs that are translationally repressed during heat stress localize to P granules, and mRNAs exit P granules as they begin translating during development (Lee et al. 2020). Similarly, translationally repressed mRNAs localize to P-bodies, and abolishing P-bodies through DDX6 depletion increases the association of P-body mRNAs with polysomes (Hubstenberger et al. 2017). Taken together, we conclude that stress granules and other RNP granules are unlikely to be significant sites of active translation relative to the surrounding cytoplasm. Future high-speed single-molecule tracking experiments will be required to definitively demonstrate the existence and extent of translation within stress granules.

Finally, the finding that a single ribosome inhibits mRNA localization to stress granules suggests a broader role for uORFs and monosomes in preventing RNA condensation in diverse biological contexts. mRNA translation in monosomes is prevalent in unicellular organisms such as baker's yeast (where ~75% of all mRNAs associate with one ribosome) (Heyer and Moore 2016), in specific tissues (Hopes et al. 2022), during nutrient deprivation (Schneider et al. 2022), and in neurons (Biever et al. 2020). Many transcripts in neuronal projections are stored in a translationally repressed state and undergo local translation in response to signaling events and extracellular cues. Intriguingly, uORF-containing transcripts are enriched in monosome fractions purified from neuronal projections (Glock et al. 2020). These results suggest not only that P-eIF2α can regulate neuronal gene expression at synapses (Glock et al. 2020), which is implicated in learning and memory (Costa-Mattioli et al. 2005, 2007; Moon et al. 2018; Sharma et al. 2020), but also that uORFs could inhibit mRNA condensation in neurons where many mRNAs are stored in a translationally inactive state. The need to store mRNAs in a translationally repressed state could make neuronal mRNAs poised to

condense, which could contribute to the aberrant assembly of RNA–protein inclusion bodies as observed in neurodegenerative contexts. uORF-mediated recruitment of ribosomes would be expected to inhibit mRNA condensation in these small subcellular compartments. Thus, our observations suggest a second role of uORFs in suppressing mRNA condensation in addition to their regulatory roles in translation in diverse organisms and contexts.

Limitations of the study

Although this study demonstrates that ribosome association inhibits uORF-containing mRNAs from localizing to stress granules, it does not evaluate the impacts of mRNA length, RNA binding protein interactions, or other potential mediators of stress-induced gene mRNA–stress granule interactions. Furthermore, it remains unclear whether proteins associating with ribosomes or changes in mRNA structure or interactions due to ribosome association limit mRNA recruitment to stress granules. Although this work provides evidence that stress-induced gene mRNAs are inhibited from localizing to stress granules through their association with ribosomes, future studies must be performed to define the role, if any, of stress granules in regulating stress-induced gene expression.

Materials and methods

Cell culture and treatments

U-2 OS cells (female osteosarcoma) were maintained in Dulbecco's modified Eagle medium (DMEM; Fisher Scientific) with 9% fetal bovine essence (FBE; Avantor), 1% streptomycin/penicillin (Gibco), and 1% glutamax (Gibco) at 37°C and 5% CO_2. U-2 OS cells stably expressing GFP-G3BP1 (Burke et al. 2020) were used to detect stress granules as described by Kedersha et al. (2008) for all experiments except the harringtonine assay using U-2 OS cells stably expressing mRuby2-PABPC1 (Burke et al. 2020). Cells were periodically confirmed negative for mycoplasma by Hoechst staining and authenticated by morphological assessment. Cells were stressed with sodium arsenite (Ricca Chemicals) at 250 µM in complete growth medium for 45 min before fixation unless noted otherwise. Small molecule inhibitors of translation used were 1 µM rocaglamide A (Fisher Scientific), 2 µg/mL harringtonine (Cayman Chemical Company), 2 µg/mL puromycin (Fisher Scientific), and 45 µM emetine (Sigma-Aldrich), which were added 10 min before fixation for smFISH experiments or added for 45 min with arsenite in stress granule analysis experiments.

Generation of uORF reporter cell lines

Oligonucleotides for *ATF4* and *GADD34* WT and mutant uORF reporter constructs upstream of the humanized Renilla luciferase (Twist Biosciences) (Supplemental Table S1) were resuspended to 25 ng/µL in molecular biology-grade water. Each start codon (ATG and Met) in the 5′ UTR of *ATF4* and *GADD34* was mutated (GCC and Ala) to ablate uORFs. Oligos were inserted in an HP138-neo backbone through Gibson Assembly (NEBuilder HiFi DNA assembly master mix). HP138-neo was a gift from Iain Cheeseman (Addgene plasmid 134247, http://n2t.net/addgene:134247, RRID: Addgene_134247) (McKinley et al. 2015). NEB stable *Escherichia coli* were prepared and transformed using Zymo Mix & Go! according to the manufacturer's instructions. Constructs were nucleofected with a helper plasmid containing a hyperactive transposase in U-2 OS cells stably expressing GFP-G3BP1. Nucleofection was performed using a Lonza 4D nucleofector and the nucleofector solution set SE for cell lines. Briefly, 2.5×10^5 cells were pelleted and resuspended in a solution containing 16.4 µL if solution SE, 3.6 µL of supplement 1, 100 ng of a helper transpose construct, and 300–500 ng of individual uORF reporter constructs. Cells were nucleofected using the Lonza 4D nucleofector using the "U2OS" cell type code and "CM104" cell code. After nucleofection, cells were resuspended with prewarmed media and selected with 400 µg/mL G418. Reporters were induced with 200 ng/mL doxycycline 24 h prior to experiments.

smFISH

smFISH was done as described previously (Dunagin et al. 2015; Khong et al. 2017) and according to Stellaris protocols. Briefly, probes (Supplemental Table S2) for *GAPDH*, *EPRS1*, *JUN*, *IFRD1*, *ACTB*, *UCP2*, *AHNAK*, *GADD34*, and luciferase were designed using Stellaris Probe Designer (version 4.2) with a masking level of 5, an oligo length of 20, and a minimum spacing length of 2 nt. *ATF4* was made using the same software; however, a mask of 4 was used to ensure a sufficient number of probes. Probes to *HSPA1A* and *HSPA1B* were described previously by Moon et al. (2020), and probes to *AHNAK* and *NORAD* were described previously by Khong et al. (2017). Probes were ordered in 96 well plate format from IDT, and equal molar amounts of each were pooled. Probe sequences are reported in Supplemental Table S2. Probe pools were labeled with either a 5-propargylamino-2′,3′-di-deoxyuridine-5′-triphosphate (ddUTP) ATTO-633 (Jena Bioscience) or ddUTP-ATTO-565 (Jena Bioscience) using terminal deoxytransferase (Thermo Scientific). Labeling reactions were performed for 16–24 h at 37°C in a thermocycler. Labeled oligos were isolated using the oligo clean and concentrate kit (Zymo) and adjusted to 12.5 µM. The degree of labeling was determined by calculating the concentration of DNA and the labeled fluorophore using a DeNovix DS-11^+ spectrophotometer after cleanup, and probes were used if >80% of the probe set was labeled. After treatments, cells were washed once with PBS and fixed in 4% paraformaldehyde for 10 min. Cells were permeabilized in 0.1% Triton X-100 in PBS with Ribolock RNase inhibitor (Thermo Fisher) for 5 min and washed twice with wash buffer A (10% formamide in 2× SSC). Cells were incubated with each probe in hybridization buffer (10% [w/v] dextran

sulfate in 10% formamide in 2× SSC) Dunagin et al. 2015) for 16 h at 37°C, protected from light. Following hybridization, cells were washed once with wash buffer A with NucBlue stain (Thermo Fisher Scientific) for 30 min and then incubated for 30 min in wash buffer A. Samples were imaged in 2× SSC.

Image acquisition and analysis of smFISH images

Images were acquired in HILO (Tokunaga et al. 2008) using an iLas2 ring-TIRF (Gataca Systems) Nikon Ti2-E microscope system with a 100× oil objective and an Andor Life 888 EMCCD camera. Z-stacks (11 per sample in 200 nm increments) were acquired, and images were deconvolved using Nikon NIS-Elements software. Laser intensity was kept constant for each channel across conditions of each experimental replicate. Representative images were deconvolved with a Richardson–Lucy deconvolution using default settings in Nikon Elements, and maximum intensity projections with brightness and contrast adjusted for clarity in ImageJ/Fiji are shown. Nondeconvolved raw image files were analyzed using a modified BigFISH/FISH-Quant (v0.6.2) pipeline (Imbert et al. 2022). To calculate total smFISH spots and colocalization of mRNA with stress granules, a local normalization filter (40 pixels × 40 pixels, 3 standard deviations) (Sage and Unser 2001) was used on the GFP (stress granule) channel to aid in watershed segmentation of stress granules for each image. Stress granules were defined to have an area >200 nm and a threshold of 45,000, which was verified by eye to have accurately segmented stress granules after filtering (Supplemental Fig. S3). Nuclei were segmented using a pretrained U-net model available from BigFISH using TensorFlow (v2.3.0) (Abadi et al. 2016). Cell segmentation was done using a watershed method. Thresholds of smFISH spots were calculated for each experimental replicate and kept constant across conditions. Counts of cytoplasmic- and stress granule-localized smFISH spots were obtained for all images after validation by eye of proper cytoplasmic and stress granule segmentation. The percentage of RNA in stress granules was calculated using cytoplasmic- and stress granule-localized RNA counts. In general, nine cells were quantified for each condition from three frames per independent experimental replicate for a total of 27 cells quantified per experiment. Statistical significance was determined using one-way ANOVA tests.

Stress granule areas were calculated from images from the *ACTB* and *IFRD1* smFISH experiments. The local normalized stress granule channel was thresholded in ImageJ/Fiji using the same threshold for every image (nine total for each condition and three independent replicates). Area was measured using the analyze particles function, with the minimum and maximum stress granule sizes set to 200 nm^2 and 5 μm^2, respectively (DMSO: $n = 2099$ stress granules, rocaglamide A: $n = 2090$ stress granules, puromycin: $n = 1853$ stress granules, harringtonine: $n = 1814$ stress granule, and emetine: $n = 1703$ stress granules). Statistical significance was determined using one-way ANOVA tests.

RNA abundance measurements by RT-qPCR

Total RNA was collected using the Zymo Quick-RNA minipreparation kit following the manufacturer's instructions. cDNA synthesis was done by using equal amounts of RNA and performing reverse transcription using the LunaScript RT SuperMix kit following the manufacturer's instructions. Luna Universal qPCR master mix was used for qPCR, and acquisition was done on the Azure Cielo qPCR machine. Analysis was done by using the Pfaffl method (Pfaffl 2001) to account for primer efficiency differences between primer sets. Primers were only used if they had efficiency values between 95% and 105%. Results are plotted as relative abundance of mRNA using *GAPDH* as a reference gene. Three independent experiments were performed, and statistical significance was determined by one-way ANOVAs. Primers for qPCR are given in Supplemental Table S3.

Polysome profiling and RT-qPCR

Polysome profiling was done as described previously (Meller et al. 2020). Briefly, cells were treated with 100 µg/mL cycloheximide for 5 min at 37°C and 5% CO_2 prior to collection. For harringtonine runoff experiments, cells were pretreated with 2 µg/mL harringtonine or DMSO for 10 or 30 min prior to a 5 min cycloheximide treatment. Cells were washed once with ice-cold PBS with 100 µg/mL cycloheximide. Cells were scraped into lysis buffer (25 mM HEPES at pH 6.9, 1% Triton X-100, 100 mM KCl, 10 mM $MgCl_2$, 100 µg/mL cycloheximide, 1 mM DTT, EDTA-free protease inhibitor cocktail [Roche], RiboLock RNase inhibitor [Thermo Fisher]). Membrane disruption was performed by passing lysate 10 times through a 25 gauge needle. Lysates were cleared by centrifugation at 20,000 rcf for 10 min at 4°C. Sucrose solutions were prepared in 25 mM HEPES (pH 6.9), 100 mM KCl, 5 mM $MgCl_2$, and 10% or 50% sucrose. Cycloheximide (100 µg/mL) and 1 mM DTT were added immediately before generating sucrose gradients. Sucrose gradients of 10%–50% sucrose were prepared using the BioComp gradient master according to the manufacturer's instructions. Equal volumes of lysate were loaded onto sucrose gradients to perform density separation on a Thermo Scientific WX-80$^+$ ultracentrifuge with a TH-641 swinging bucket rotor. Sucrose gradients were spun at 40,000 rpm for 3 h at 4°C. UV (A260) polysome profiles were obtained using the Triax flowcell (BioComp Instruments). Polysome to monosome ratios were calculated by measuring the area under the curve using the scipy (v1.12.0) trapezoid integration function. Twelve fractions were collected for each sample. RNA isolation from sucrose gradients was done using Trizol LS/chloroform extraction following the manufacturer's instructions. Equal volumes of RNA from fractions were used for reverse transcription using LunaScript RT SuperMix (New England Biolabs). RT-qPCR was performed as described above. Analysis of qPCR data was done as described previously (Panda et al. 2017), and the percentage of RNA in each fraction was determined by normalizing to fraction 1. Free

fractions were defined as fractions 1–5, which represent the free RNP peak, 40S ribosomal subunit, and 60S ribosomal subunit. Light polysomes were defined as fractions 6–9, which represent one or two ribosomes. Heavy polysomes were defined as fractions 10–12, which represent three or more ribosomes.

Ribo-seq analysis

Ribo-seq data that were previously published (Andreev et al. 2015) were reanalyzed with Trips-Viz (Kiniry et al. 2021), and single-transcript comparison plots were generated for RNAs of interest with default settings. Ambiguous reads were allowed for *HSPA1A*, *HSPA1B*, and *GAPDH*. Transcript IDs were obtained from NCBI as follows: ENST00000337304 (*ATF4*), ENST00000 200453 (*GADD34*), ENST00000366923 (*EPRS1*), ENST 00000375651 (*HSPA1A*), ENST00000375650 (*HSPA1B*), ENST00000371222 (*JUN*), ENST00000396858 (*GAPDH*), ENST00000378024 (*AHNAK*), and ENST00000565493 (*NORAD*).

Live-cell imaging, immunofluorescence, and analysis of stress granules

U-2 OS cells stably expressing GFP-G3BP1 or mRuby2-PABPC1 plated on glass-bottom dishes were treated with 2 µg/mL harringtonine in DMSO or 50 µM lactimidomycin in DMSO or an equal volume of DMSO (0.1% or 0.5%) for 30 min in complete fluorobrite medium (Thermo Fisher Scientific). Arsenite was added to reach 250 µM, and images were acquired every minute with a widefield fluorescence Nikon Ti2-E microscope system equipped with a Lumencor Spectra III light engine using a 40× objective and an Andor Life 888 EMCCD camera for 1 h at 37°C and 5% CO_2. Harringtonine washout experiments were performed by treating cells with harringtonine for 30 min followed by either washing out all media three times and replacing with media containing 250 µM arsenite or adding arsenite directly to the cells to reach 250 µM. After imaging of cells treated with DMSO or harringtonine in the presence or absence of arsenite, cells were washed in PBS and fixed with 4% paraformaldehyde for 10 min. Cells were washed twice with PBS, and sequential immunofluorescence and FISH were done following Stellaris protocols. Briefly, cells were permeabilized in 0.1% Tween-20 in PBS with RiboLock RNase inhibitor (Thermo Fisher Scientific) for 10 min. Cells were washed with PBS and incubated with primary UBAP2L antibody (Cell Signaling Technology 40199S) in PBS for 1 h at room temperature with rocking. Cells were washed three times with PBS and incubated with secondary anti-rabbit 647 or 405 for 1 h at room temperature. Cells were washed three times with PBS and fixed again with 4% paraformaldehyde for 10 min at room temperature. After fixation, cells were incubated with 1:400 Cy3-oligo(dT) probes (IDT) in hybridization buffer for 16 h at 37°C, protected from light. Cells were washed twice with wash buffer A and imaged in 2× SSC as described above for smFISH data acquisition.

Quantification of stress granules from live-cell imaging was done using the ImageJ/Fiji cell counter plug-in (Schindelin et al. 2012) for every 10 frames to determine the average percentage of cells with stress granules. Results are presented as the average ± SEM percentage of cells in each condition that were positive for stress granules ($n = 3$ for all times and conditions, except the DMSO 20 min time point, which was $n = 2$). Line scans were done in ImageJ/Fiji using the plot profile function (Schindelin et al. 2012) on the fixed-cell images from the harringtonine GFP-G3BP1 pretreatment experiment ($n = 2$ independent experiments) (Fig. 3F; Supplemental Fig. S4; Schindelin et al. 2012). Quantification of GFP-G3BP1 foci and the cytoplasmic area in the fixed-cell images was done in ImageJ/Fiji using the analyze particles function with the minimum size being 200 nm^2, and the percentage of cytoplasmic area occupied by stress granules is reported from $n = 18$–19 cells.

Widefield image acquisition and analysis of stress granules

U-2 OS cells stably expressing GFP-G3BP1 were untreated or treated with 250 µM arsenite, 0.1% DMSO, 1 µM rocaglamide A, 2 µg/mL puromycin, 2 µg/mL rocaglamide A and 2 µg/mL puromycin, 2 µg/mL harringtonine, 2 µM harringtonine and 2 µM puromycin, or 45 µM emetine for 45 min. Cells were fixed in 4% PFA for 10 min and washed twice with PBS. During the second wash, nuclei were stained with NucBlue stain (Thermo Fisher Scientific) for 30 min. Images were acquired using an EVOS M5000 imaging system with 470/525 nm GFP and 357/447 nm DAPI LED light cubes and a CMOS monochrome camera with a 40× objective. Three frames per condition were captured for each of the three independent experimental replicates (66–192 cells were counted per replicate). Quantification was done using the ImageJ/Fiji cell counter plug-in (Schindelin et al. 2012) in each frame to determine the average percentage of cells with stress granules. Results are presented as the average ± SEM percentage of cells in each condition that were positive for stress granules.

Western blot analysis

To assess protein levels during arsenite treatment time-course experiments, equal numbers of U-2 OS cells were incubated in the absence or presence of 250 µM arsenite for 15, 30, or 45 min. Cells were lysed in RIPA buffer (25 mM Tris HCl at pH 7.5, 300 mM NaCl, 2% NP-40 substitute, 2% sodium deoxycholate, 0.2% SDS) supplemented with HALT protease/phosphatase inhibitor cocktail (Thermo Fisher Scientific) and benzonase nuclease (Sigma) immediately before collection. Equal volumes of lysate were loaded onto Bolt 4%–12% Bis-Tris Plus gel and run in MES running buffer (50 mM Tris, 50 mM MES, 0.1% SDS, 1 mM EDTA at pH 7.3). Proteins were transferred to a PVDF membrane, and total protein was detected with Azure Total protein Q stain. Membranes were blocked in 5% milk in TBST and then probed for

GAPDH (Thermo Fisher Scientific MA5-15738-D680), ATF4 (Proteintech 81798-1-RR), EPRS1 (Proteintech 67712-1-IG), GADD34 (Proteintech 81250-1-RR), JUN (Proteintech 66313-1-IG), or HSP70 (Proteintech 10995-1-AP). Primary antibodies were used at 1:1000 dilutions. Membranes were washed three times with TBST followed by a 1 h incubation at room temperature with antirabbit (Cell Signaling Technology 7074S) or antimouse (Cell Signaling Technology 7076S) HRP-conjugated secondary antibodies for ATF4 and GADD34, antimouse Dylight800 (Thermo Fisher Scientific SA5-35521) for EPRS1 and JUN, and antirabbit Dylight680 (Thermo Fisher Scientific 35568) secondary antibodies for HSP70 at 1:5000 dilutions in 5% milk in TBST. Membranes were washed three times with TBST, and fluorescent signal was detected on the Azure C600 imager. ATF4 and GADD34 were detected using SuperSignal West ATTO following the manufacturer's instructions with the Azure C600 imager using the chemiluminescent setting. Relative protein abundances normalized to total protein are reported from three independent experiments. One-way ANOVA tests were done to assess significance.

Quantification and statistical analysis

Statistical details of all experiments are provided in the figure legends and the Materials and Methods. If not noted otherwise, the average ± SEM is shown for each experiment. Significance was defined as $P \leq 0.05$ for all experiments using one-way ANOVA tests. Plotting and data analysis were done in R or Python using the following packages: ggplot2 (Wickham 2016), tidyR (Wickham et al. 2019), dplyR (Wickham et al. 2019), pandas, numpy (Harris et al. 2020), and matplotlib (Hunter 2007).

Data availability

Additional information and requests for resources and reagents fulfilled on request. All unique reagents generated in this study are available without restrictions for academic research purposes. Supplemental Table S4 contains all source data. This study does not report original code.

Competing interests statement

The authors declare no competing interests.

Acknowledgments

We thank all members of the Moon laboratory for helpful discussions. GFP-G3BP1 and mRuby2-PABPC1 U-2 OS cells were kindly provided by James Burke and Roy Parker. We thank David Burke for technical advice, and Tony Antonellis and John Moran for critical feedback. We thank Iain Cheeseman for sharing the HP138-neo plasmid. N.S.H. was supported in part by the Michigan Predoctoral Training in Genetics T32 (5T32GM007544 and T32GM149391). This research was supported by grant awards to S.L.M. from the National Institute of General Medical Sciences (R35GM146711) and the Chan Zuckerberg Initiative.

Author contributions: N.S.H., B.D., and S.L.M. conceived the study. N.S.H. and B.D. curated the data. N.S.H. performed the formal analysis. N.S.H. and S.L.M. acquired the funding. N.S.H. performed the investigation. N.S.H., B.D., and S.L.M. performed the methodology. N.S.H., B.D., and S.L.M. were the project adminstrators. B.D. and S.L.M. acquired the resources. N.S.H. operated the software. S.L.M. supervised the study. N.S.H. validated the results. N.S.H. and S.L.M. visualized the study. N.S.H. and S.L.M. wrote the original draft of the manusctipt. N.S.H., B.D., and S.L.M. reviewed and edited the manuscript.

References

Abadi M, Barham P, Chen J, Chen Z, Davis A, Dean J, Devin M, Ghemawat S, Irving G, Isard M, et al. 2016. TensorFlow: a system for large-scale machine learning. *OSDI'16: Proceedings of the 12th USENIX Symposium on Operating Systems Design and Implementation*, pp. 265–283. USENIX Association, San Francisco. https://www.usenix.org/system/files/conference/osdi16/osdi16-abadi.pdf

Abastado JP, Miller PF, Jackson BM, Hinnebusch AG. 1991. Suppression of ribosomal reinitiation at upstream open reading frames in amino acid-starved cells forms the basis for *GCN4* translational control. *Mol Cell Biol* **11:** 486–496. doi:10.1128/mcb.11.1.486-496.1991

Adivarahan S, Livingston N, Nicholson B, Rahman S, Wu B, Rissland OS, Zenklusen D. 2018. Spatial organization of single mRNPs at different stages of the gene expression pathway. *Mol Cell* **72:** 727–738.e5. doi:10.1016/j.molcel.2018.10.010

Adjibade P, St-Sauveur VG, Quevillon Huberdeau M, Fournier M-J, Savard A, Coudert L, Khandjian EW, Mazroui R. 2015. Sorafenib, a multikinase inhibitor, induces formation of stress granules in hepatocarcinoma cells. *Oncotarget* **6:** 43927–43943. doi:10.18632/oncotarget.5980

Andreev DE, O'Connor PBF, Fahey C, Kenny EM, Terenin IM, Dmitriev SE, Cormican P, Morris DW, Shatsky IN, Baranov PV. 2015. Translation of 5′ leaders is pervasive in genes resistant to eIF2 repression. *eLife* **4:** e03971. doi:10.7554/eLife.03971

Asadi MR, Sadat Moslehian M, Sabaie H, Jalaiei A, Ghafouri-Fard S, Taheri M, Rezazadeh M. 2021. Stress granules and neurodegenerative disorders: a scoping review. *Front Aging Neurosci* **13:** 650740. doi:10.3389/fnagi.2021.650740

Banani SF, Rice AM, Peeples WB, Lin Y, Jain S, Parker R, Rosen MK. 2016. Compositional control of phase-separated cellular bodies. *Cell* **166:** 651–663. doi:10.1016/j.cell.2016.06.010

Baron DM, Matheny T, Lin Y-C, Leszyk JD, Kenna K, Gall KV, Santos DP, Tischbein M, Funes S, Hayward LJ, et al. 2019. Quantitative proteomics identifies proteins that resist translational repression and become dysregulated in ALS-FUS. *Hum Mol Genet* **28:** 2143–2160. doi:10.1093/hmg/ddz048

Baymiller M, Moon SL. 2023. Stress granules as causes and consequences of translation suppression. *Antioxid Redox Signal* **39:** 390–409. doi:10.1089/ars.2022.0164

Behrens A, Sibilia M, Wagner EF. 1999. Amino-terminal phosphorylation of c-Jun regulates stress-induced apoptosis and cellular proliferation. *Nat Genet* **21:** 326–329. doi:10.1038/6854

Biever A, Glock C, Tushev G, Ciirdaeva E, Dalmay T, Langer JD, Schuman EM. 2020. Monosomes actively translate synaptic mRNAs in neuronal processes. *Science* **367:** eaay4991. doi:10.1126/science.aay4991

Bounedjah O, Desforges B, Wu T-D, Pioche-Durieu C, Marco S, Hamon L, Curmi PA, Guerquin-Kern J-L, Piétrement O, Pastré D. 2014. Free mRNA in excess upon polysome dissociation is a scaffold for protein multimerization to form stress granules. *Nucleic Acids Res* **42:** 8678–8691. doi:10.1093/nar/gku582

Boyce M, Bryant KF, Jousse C, Long K, Harding HP, Scheuner D, Kaufman RJ, Ma D, Coen DM, Ron D, et al. 2005. A selective inhibitor of eIF2α dephosphorylation protects cells from ER stress. *Science* **307:** 935–939. doi:10.1126/science.1101902

Brar GA, Weissman JS. 2015. Ribosome profiling reveals the what, when, where and how of protein synthesis. *Nat Rev Mol Cell Biol* **16:** 651–664. doi:10.1038/nrm4069

Brar GA, Yassour M, Friedman N, Regev A, Ingolia NT, Weissman JS. 2012. High-resolution view of the yeast meiotic program revealed by ribosome profiling. *Science* **335:** 552–557. doi:10.1126/science.1215110

Brostrom CO, Brostrom MA. 1998. Regulation of translational initiation during cellular responses to stress. *Prog Nucleic Acid Res Mol Biol* **58:** 79–125. doi:10.1016/s0079-6603(08)60034-3

Buchan JR, Kolaitis R-M, Taylor JP, Parker R. 2013. Eukaryotic stress granules are cleared by autophagy and Cdc48/VCP function. *Cell* **153:** 1461–1474. doi:10.1016/j.cell.2013.05.037

Budkina K, El Hage K, Clément M-J, Desforges B, Bouhss A, Joshi V, Maucuer A, Hamon L, Ovchinnikov LP, Lyabin DN, et al. 2021. YB-1 unwinds mRNA secondary structures in vitro and negatively regulates stress granule assembly in HeLa cells. *Nucleic Acids Res* **49:** 10061–10081. doi:10.1093/nar/gkab748

Burke JM, Moon SL, Matheny T, Parker R. 2019. RNase L reprograms translation by widespread mRNA turnover escaped by antiviral mRNAs. *Mol Cell* **75:** 1203–1217.e5. doi:10.1016/j.molcel.2019.07.029

Burke JM, Lester ET, Tauber D, Parker R. 2020. RNase L promotes the formation of unique ribonucleoprotein granules distinct from stress granules. *J Biol Chem* **295:** 1426–1438. doi:10.1074/jbc.RA119.011638

Chen JJ, Throop MS, Gehrke L, Kuo I, Pal JK, Brodsky M, London IM. 1991. Cloning of the cDNA of the heme-regulated eukaryotic initiation factor 2α (eIF-2α) kinase of rabbit reticulocytes: homology to yeast GCN2 protein kinase and human double-stranded-RNA-dependent eIF-2α kinase. *Proc Natl Acad Sci* **88:** 7729–7733. doi:10.1073/pnas.88.17.7729

Chothani SP, Adami E, Widjaja AA, Langley SR, Viswanathan S, Pua CJ, Zhihao NT, Harmston N, D'Agostino G, Whiffin N, et al. 2022. A high-resolution map of human RNA translation. *Mol Cell* **82:** 2885–2899.e8. doi:10.1016/j.molcel.2022.06.023

Costa-Mattioli M, Walter P. 2020. The integrated stress response: from mechanism to disease. *Science* **368:** eaat5314. doi:10.1126/science.aat5314

Costa-Mattioli M, Gobert D, Harding H, Herdy B, Azzi M, Bruno M, Bidinosti M, Ben Mamou C, Marcinkiewicz E, Yoshida M, et al. 2005. Translational control of hippocampal synaptic plasticity and memory by the eIF2α kinase GCN2. *Nature* **436:** 1166–1170. doi:10.1038/nature03897

Costa-Mattioli M, Gobert D, Stern E, Gamache K, Colina R, Cuello C, Sossin W, Kaufman R, Pelletier J, Rosenblum K, et al. 2007. eIF2α phosphorylation bidirectionally regulates the switch from short- to long-term synaptic plasticity and memory. *Cell* **129:** 195–206. doi:10.1016/j.cell.2007.01.050

Curdy N, Lanvin O, Cerapio J-P, Pont F, Tosolini M, Sarot E, Valle C, Saint-Laurent N, Lhuillier E, Laurent C, et al. 2023. The proteome and transcriptome of stress granules and P bodies during human T lymphocyte activation. *Cell Rep* **42:** 112211. doi:10.1016/j.celrep.2023.112211

Dang Y, Kedersha N, Low W-K, Romo D, Gorospe M, Kaufman R, Anderson P, Liu JO. 2006. Eukaryotic initiation factor 2α-independent pathway of stress granule induction by the natural product pateamine A. *J Biol Chem* **281:** 32870–32878. doi:10.1074/jbc.M606149200

Decker CJ, Burke JM, Mulvaney PK, Parker R. 2022. RNA is required for the integrity of multiple nuclear and cytoplasmic membrane-less RNP granules. *EMBO J* **41:** e110137. doi:10.15252/embj.2021110137

Dever TE, Feng L, Wek RC, Cigan AM, Donahue TF, Hinnebusch AG. 1992. Phosphorylation of initiation factor 2α by protein kinase GCN2 mediates gene-specific translational control of GCN4 in yeast. *Cell* **68:** 585–596. doi:10.1016/0092-8674(92)90193-g

Dever TE, Ivanov IP, Hinnebusch AG. 2023. Translational regulation by uORFs and start codon selection stringency. *Genes Dev* **37:** 474–489. doi:10.1101/gad.350752.123

Dunagin M, Cabili MN, Rinn J, Raj A. 2015. Visualization of lncRNA by single-molecule fluorescence in situ hybridization. *Methods Mol Biol* **1262:** 3–19. doi:10.1007/978-1-4939-2253-6_1

Enam SU, Zinshteyn B, Goldman DH, Cassani M, Livingston NM, Seydoux G, Green R. 2020. Puromycin reactivity does not accurately localize translation at the subcellular level. *eLife* **9:** e60303. doi:10.7554/eLife.60303

English AM, Green KM, Moon SL. 2022. A (dis)integrated stress response: genetic diseases of eIF2α regulators. *Wiley Interdiscip Rev RNA* **13:** e1689. doi:10.1002/wrna.1689

Fedorovskiy AG, Burakov AV, Terenin IM, Bykov DA, Lashkevich KA, Popenko VI, Makarova NE, Sorokin II, Sukhinina AP, Prassolov VS, et al. 2023. A solitary stalled 80S ribosome prevents mRNA recruitment to stress granules. *Biochemistry* **88:** 1786–1799. doi:10.1134/S000629792311010X

Ferguson L, Upton HE, Pimentel SC, Mok A, Lareau LF, Collins K, Ingolia NT. 2023. Streamlined and sensitive mono- and di-ribosome profiling in yeast and human cells. *Nat Methods* **20:** 1704–1715. doi:10.1038/s41592-023-02028-1

Freibaum BD, Messing J, Nakamura H, Yurtsever U, Wu J, Kim HJ, Hixon J, Lemieux RM, Duffner J, Huynh W, et al. 2024. Identification of small molecule inhibitors of G3BP-driven stress granule formation. *J Cell Biol* **223:** e202308083. doi:10.1083/jcb.202308083

Fresno M, Jiménez A, Vázquez D. 1977. Inhibition of translation in eukaryotic systems by harringtonine. *Eur J Biochem* **72:** 323–330. doi:10.1111/j.1432-1033.1977.tb11256.x

Garshott DM, An H, Sundaramoorthy E, Leonard M, Vicary A, Harper JW, Bennett EJ. 2021. iRQC, a surveillance pathway for 40S ribosomal quality control during mRNA translation initiation. *Cell Rep* **36:** 109642. doi:10.1016/j.celrep.2021.109642

Ge Y, Jin J, Li J, Ye M, Jin X. 2022. The roles of G3BP1 in human diseases (review). *Gene* **821:** 146294. doi:10.1016/j.gene.2022.146294

Glauninger H, Bard JAM, Wong Hickernell CJ, Airoldi EM, Li W, Singer RH, Paul S, Fei J, Sosnick TR, Wallace EWJ, et al. 2024. Transcriptome-wide mRNA condensation precedes stress granule formation and excludes stress-induced transcripts. bioRxiv doi:10.1101/2024.04.15.589678

Glock C, Biever A, Tushev G, Bartnik I, Nassim-Assir B, Dieck ST, Schuman EM. 2020. The mRNA translation landscape

in the synaptic neuropil. bioRxiv doi:10.1101/2020.06.09.141960

Grollman AP. 1968. Inhibitors of protein biosynthesis. V. Effects of emetine on protein and nucleic acid biosynthesis in HeLa cells. *J Biol Chem* **243:** 4089–4094. doi:10.1016/S0021-9258(18)93283-7

Guillén-Boixet J, Kopach A, Holehouse AS, Wittmann S, Jahnel M, Schlüßler R, Kim K, Trussina IREA, Wang J, Mateju D, et al. 2020. RNA-induced conformational switching and clustering of G3BP drive stress granule assembly by condensation. *Cell* **181:** 346–361.e17. doi:10.1016/j.cell.2020.03.049

Guo Q, Wu Y, Wang X, Meng L, Liao Z, Ji W, Zhang P, Lin J. 2024. Translation landscape of stress granules. *Research Square* doi:10.21203/rs.3.rs-4497528/v1

Gupta RS, Siminovitch L. 1977. Mutants of CHO cells resistant to the protein synthesis inhibitors, cryptopleurine and tylocrebrine: genetic and biochemical evidence for common site of action of emetine, cryptopleurine, tylocrebrine, and tubulosine. *Biochemistry* **16:** 3209–3214. doi:10.1021/bi00633a026

Guzikowski AR, Chen YS, Zid BM. 2019. Stress-induced mRNP granules: form and function of processing bodies and stress granules. *Wiley Interdiscip Rev RNA* **10:** e1524. doi:10.1002/wrna.1524

Gwon Y, Maxwell BA, Kolaitis R-M, Zhang P, Kim HJ, Taylor JP. 2021. Ubiquitination of G3BP1 mediates stress granule disassembly in a context-specific manner. *Science* **372:** eabf6548. doi:10.1126/science.abf6548

Han J, Back SH, Hur J, Lin Y-H, Gildersleeve R, Shan J, Yuan CL, Krokowski D, Wang S, Hatzoglou M, et al. 2013. ER-stress-induced transcriptional regulation increases protein synthesis leading to cell death. *Nat Cell Biol* **15:** 481–490. doi:10.1038/ncb2738

Harding HP, Novoa I, Zhang Y, Zeng H, Wek R, Schapira M, Ron D. 2000. Regulated translation initiation controls stress-induced gene expression in mammalian cells. *Mol Cell* **6:** 1099–1108. doi:10.1016/s1097-2765(00)00108-8

Harris CR, Millman KJ, van der Walt SJ, Gommers R, Virtanen P, Cournapeau D, Wieser E, Taylor J, Berg S, Smith NJ, et al. 2020. Array programming with NumPy. *Nature* **585:** 357–362. doi:10.1038/s41586-020-2649-2

Heyer EE, Moore MJ. 2016. Redefining the translational status of 80S monosomes. *Cell* **164:** 757–769. doi:10.1016/j.cell.2016.01.003

Hinnebusch AG. 1997. Translational regulation of yeast GCN4: a window on factors that control initiator–tRNA binding to the ribosome. *J Biol Chem* **272:** 21661–21664. doi:10.1074/jbc.272.35.21661

Hobson BD, Kong L, Hartwick EW, Gonzalez RL, Sims PA. 2020. Elongation inhibitors do not prevent the release of puromycylated nascent polypeptide chains from ribosomes. *eLife* **9:** e60048. doi:10.7554/eLife.60048

Hopes T, Norris K, Agapiou M, McCarthy CGP, Lewis PA, O'Connell MJ, Fontana J, Aspden JL. 2022. Ribosome heterogeneity in *Drosophila melanogaster* gonads through paralog-switching. *Nucleic Acids Res* **50:** 2240–2257. doi:10.1093/nar/gkab606

Hu C, Yang J, Qi Z, Wu H, Wang B, Zou F, Mei H, Liu J, Wang W, Liu Q. 2022. Heat shock proteins: biological functions, pathological roles, and therapeutic opportunities. *MedComm* **3:** e161. doi:10.1002/mco2.161

Huang MT. 1975. Harringtonine, an inhibitor of initiation of protein biosynthesis. *Mol Pharmacol* **11:** 511–519. doi:10.1016/S0026-895X(25)10662-7

Hubstenberger A, Courel M, Bénard M, Souquere S, Ernoult-Lange M, Chouaib R, Yi Z, Morlot J-B, Munier A, Fradet M, et al. 2017. P-body purification reveals the condensation of repressed mRNA regulons. *Mol Cell* **68:** 144–157.e5. doi:10.1016/j.molcel.2017.09.003

Hunter JD. 2007. Matplotlib: a 2D graphics environment. *Comput Sci Eng* **9:** 90–95. doi:10.1109/MCSE.2007.55

Hurtaud C, Gelly C, Bouillaud F, Lévi-Meyrueis C. 2006. Translation control of UCP2 synthesis by the upstream open reading frame. *Cell Mol Life Sci* **63:** 1780–1789. doi:10.1007/s00018-006-6129-0

Imbert A, Ouyang W, Safieddine A, Coleno E, Zimmer C, Bertrand E, Walter T, Mueller F. 2022. FISH-quant v2: a scalable and modular tool for smFISH image analysis. *RNA* **28:** 786–795. doi:10.1261/rna.079073.121

Ingolia NT, Lareau LF, Weissman JS. 2011. Ribosome profiling of mouse embryonic stem cells reveals the complexity and dynamics of mammalian proteomes. *Cell* **147:** 789–802. doi:10.1016/j.cell.2011.10.002

Ingolia NT, Brar GA, Rouskin S, McGeachy AM, Weissman JS. 2012. The ribosome profiling strategy for monitoring translation in vivo by deep sequencing of ribosome-protected mRNA fragments. *Nat Protoc* **7:** 1534–1550. doi:10.1038/nprot.2012.086

Irgen-Gioro S, Yoshida S, Walling V, Chong S. 2022. Fixation can change the appearance of phase separation in living cells. *eLife* **11:** e79903. doi:10.7554/eLife.79903

Ishimura R, Nagy G, Dotu I, Chuang JH, Ackerman SL. 2016. Activation of GCN2 kinase by ribosome stalling links translation elongation with translation initiation. *eLife* **5:** e14295. doi:10.7554/eLife.14295

Iwasaki S, Floor SN, Ingolia NT. 2016. Rocaglates convert DEAD-box protein eIF4A into a sequence-selective translational repressor. *Nature* **534:** 558–561. doi:10.1038/nature17978

Iwasaki S, Iwasaki W, Takahashi M, Sakamoto A, Watanabe C, Shichino Y, Floor SN, Fujiwara K, Mito M, Dodo K, et al. 2019. The translation inhibitor rocaglamide targets a bimolecular cavity between eIF4A and polypurine RNA. *Mol Cell* **73:** 738–748.e9. doi:10.1016/j.molcel.2018.11.026

Jain S, Wheeler JR, Walters RW, Agrawal A, Barsic A, Parker R. 2016. ATPase-modulated stress granules contain a diverse proteome and substructure. *Cell* **164:** 487–498. doi:10.1016/j.cell.2015.12.038

Jia X, Zhang S, Tan S, Du B, He M, Qin H, Chen J, Duan X, Luo J, Chen F, et al. 2022. De novo variants in genes regulating stress granule assembly associate with neurodevelopmental disorders. *Sci Adv* **8:** eabo7112. doi:10.1126/sciadv.abo7112

Kedersha N, Anderson P. 2002. Stress granules: sites of mRNA triage that regulate mRNA stability and translatability. *Biochem Soc Trans* **30:** 963–969. doi:10.1042/bst0300963

Kedersha NL, Gupta M, Li W, Miller I, Anderson P. 1999. RNA-binding proteins TIA-1 and TIAR link the phosphorylation of eIF-2α to the assembly of mammalian stress granules. *J Cell Biol* **147:** 1431–1442. doi:10.1083/jcb.147.7.1431

Kedersha N, Cho MR, Li W, Yacono PW, Chen S, Gilks N, Golan DE, Anderson P. 2000. Dynamic shuttling of Tia-1 accompanies the recruitment of mRNA to mammalian stress granules. *J Cell Biol* **151:** 1257–1268. doi:10.1083/jcb.151.6.1257

Kedersha N, Chen S, Gilks N, Li W, Miller IJ, Stahl J, Anderson P. 2002. Evidence that ternary complex (eIF2–GTP–$tRNA_i^{Met}$)–deficient preinitiation complexes are core constituents of mammalian stress granules. *Mol Biol Cell* **13:** 195–210. doi:10.1091/mbc.01-05-0221

Kedersha N, Tisdale S, Hickman T, Anderson P. 2008. Real-time and quantitative imaging of mammalian stress granules and processing bodies. *Methods Enzymol* **448:** 521–552. doi:10.1016/S0076-6879(08)02626-8

Kedersha N, Panas MD, Achorn CA, Lyons S, Tisdale S, Hickman T, Thomas M, Lieberman J, McInerney GM, Ivanov P, et al. 2016. G3BP–Caprin1–USP10 complexes mediate stress granule condensation and associate with 40S subunits. *J Cell Biol* **212:** 845–860. doi:10.1083/jcb.201508028

Khong A, Parker R. 2018. mRNP architecture in translating and stress conditions reveals an ordered pathway of mRNP compaction. *J Cell Biol* **217:** 4124–4140. doi:10.1083/jcb.201806183

Khong A, Matheny T, Jain S, Mitchell SF, Wheeler JR, Parker R. 2017. The stress granule transcriptome reveals principles of mRNA accumulation in stress granules. *Mol Cell* **68:** 808–820.e5. doi:10.1016/j.molcel.2017.10.015

Kiniry SJ, Judge CE, Michel AM, Baranov PV. 2021. Trips-Viz: an environment for the analysis of public and user-generated ribosome profiling data. *Nucleic Acids Res* **49:** W662–W670. doi:10.1093/nar/gkab323

Kozak M. 1987. An analysis of 5′-noncoding sequences from 699 vertebrate messenger RNAs. *Nucleic Acids Res* **15:** 8125–8148. doi:10.1093/nar/15.20.8125

Lee Y-Y, Cevallos RC, Jan E. 2009. An upstream open reading frame regulates translation of GADD34 during cellular stresses that induce eIF2α phosphorylation. *J Biol Chem* **284:** 6661–6673. doi:10.1074/jbc.M806735200

Lee S, Liu B, Lee S, Huang S-X, Shen B, Qian S-B. 2012. Global mapping of translation initiation sites in mammalian cells at single-nucleotide resolution. *Proc Natl Acad Sci* **109:** E2424–E2432. doi:10.1073/pnas.1207846109

Lee C-YS, Putnam A, Lu T, He S, Ouyang JPT, Seydoux G. 2020. Recruitment of mRNAs to P granules by condensation with intrinsically-disordered proteins. *eLife* **9:** e52896. doi:10.7554/eLife.52896

Lee M, Moon HC, Jeong H, Kim DW, Park HY, Shin Y. 2024. Optogenetic control of mRNA condensation reveals an intimate link between condensate material properties and functions. *Nat Commun* **15:** 3216. doi:10.1038/s41467-024-47442-x

Li L, Garg M, Wang Y, Wang W, Godbout R. 2022. DEAD box 1 (DDX1) protein binds to and protects cytoplasmic stress response mRNAs in cells exposed to oxidative stress. *J Biol Chem* **298:** 102180. doi:10.1016/j.jbc.2022.102180

Liboy-Lugo JM, Espinoza CA, Sheu-Gruttadauria J, Park JE, Xu A, Jowhar Z, Gao AL, Carmona-Negrón JA, Wittmann T, Jura N, et al. 2024. G3BP isoforms differentially affect stress granule assembly and gene expression during cellular stress. *Mol Biol Cell* **35:** ar140. doi:10.1091/mbc.E24-02-0062

Lines CL, McGrath MJ, Dorwart T, Conn CS. 2023. The integrated stress response in cancer progression: a force for plasticity and resistance. *Front Oncol* **13:** 1206561. doi:10.3389/fonc.2023.1206561

Liu B, Qian S-B. 2016. Characterizing inactive ribosomes in translational profiling. *Translation* **4:** e1138018. doi:10.1080/21690731.2015.1138018

Markmiller S, Soltanieh S, Server KL, Mak R, Jin W, Fang MY, Luo E-C, Krach F, Yang D, Sen A, et al. 2018. Context-dependent and disease-specific diversity in protein interactions within stress granules. *Cell* **172:** 590–604.e13. doi:10.1016/j.cell.2017.12.032

Marlin E, Viu-Idocin C, Arrasate M, Aragón T. 2022. The role and therapeutic potential of the integrated stress response in amyotrophic lateral sclerosis. *Int J Mol Sci* **23:** 7823. doi:10.3390/ijms23147823

Mateju D, Eichenberger B, Voigt F, Eglinger J, Roth G, Chao JA. 2020. Single-molecule imaging reveals translation of mRNAs localized to stress granules. *Cell* **183:** 1801–1812.e13. doi:10.1016/j.cell.2020.11.010

Matheny T, Rao BS, Parker R. 2019. Transcriptome-wide comparison of stress granules and P-bodies reveals that translation plays a major role in RNA partitioning. *Mol Cell Biol* **39:** e00313-19. doi:10.1128/MCB.00313-19

Matheny T, Van Treeck B, Huynh TN, Parker R. 2021. RNA partitioning into stress granules is based on the summation of multiple interactions. *RNA* **27:** 174–189. doi:10.1261/rna.078204.120

Matsui M, Yachie N, Okada Y, Saito R, Tomita M. 2007. Bioinformatic analysis of post-transcriptional regulation by uORF in human and mouse. *FEBS Lett* **581:** 4184–4188. doi:10.1016/j.febslet.2007.07.057

McGillivray P, Ault R, Pawashe M, Kitchen R, Balasubramanian S, Gerstein M. 2018. A comprehensive catalog of predicted functional upstream open reading frames in humans. *Nucleic Acids Res* **46:** 3326–3338. doi:10.1093/nar/gky188

McKinley KL, Sekulic N, Guo LY, Tsinman T, Black BE, Cheeseman IM. 2015. The CENP–L–N complex forms a critical node in an integrated meshwork of interactions at the centromere–kinetochore interface. *Mol Cell* **60:** 886–898. doi:10.1016/j.molcel.2015.10.027

Meller A, Coombs D, Shalgi R. 2020. Fluorescent polysome profiling reveals stress-mediated regulation of HSPA14–ribosome interactions. bioRxiv doi:10.1101/860833

Moon SL, Parker R. 2018. *EIF2B2* mutations in vanishing white matter disease hypersuppress translation and delay recovery during the integrated stress response. *RNA* **24:** 841–852. doi:10.1261/rna.066563.118

Moon SL, Sonenberg N, Parker R. 2018. Neuronal regulation of eIF2α function in health and neurological disorders. *Trends Mol Med* **24:** 575–589. doi:10.1016/j.molmed.2018.04.001

Moon SL, Morisaki T, Khong A, Lyon K, Parker R, Stasevich TJ. 2019. Multicolour single-molecule tracking of mRNA interactions with RNP granules. *Nat Cell Biol* **21:** 162–168. doi:10.1038/s41556-018-0263-4

Moon SL, Morisaki T, Stasevich TJ, Parker R. 2020. Coupling of translation quality control and mRNA targeting to stress granules. *J Cell Biol* **219:** e202004120. doi:10.1083/jcb.202004120

Namkoong S, Ho A, Woo YM, Kwak H, Lee JH. 2018. Systematic characterization of stress-induced RNA granulation. *Mol Cell* **70:** 175–187.e8. doi:10.1016/j.molcel.2018.02.025

Nathans D. 1964. Puromycin inhibition of protein synthesis: incorporation of puromycin into peptide chains. *Proc Natl Acad Sci* **51:** 585–592. doi:10.1073/pnas.51.4.585

Neill G, Masson GR. 2023. A stay of execution: ATF4 regulation and potential outcomes for the integrated stress response. *Front Mol Neurosci* **16:** 1112253. doi:10.3389/fnmol.2023.1112253

Nover L, Scharf KD, Neumann D. 1983. Formation of cytoplasmic heat shock granules in tomato cell cultures and leaves. *Mol Cell Biol* **3:** 1648–1655. doi:10.1128/mcb.3.9.1648-1655.1983

Nover L, Scharf KD, Neumann D. 1989. Cytoplasmic heat shock granules are formed from precursor particles and are associated with a specific set of mRNAs. *Mol Cell Biol* **9:** 1298–1308. doi:10.1128/mcb.9.3.1298-1308.1989

Novoa I, Zeng H, Harding HP, Ron D. 2001. Feedback inhibition of the unfolded protein response by *GADD34*-mediated dephosphorylation of eIF2α. *J Cell Biol* **153:** 1011–1022. doi:10.1083/jcb.153.5.1011

Novoa I, Zhang Y, Zeng H, Jungreis R, Harding HP, Ron D. 2003. Stress-induced gene expression requires programmed recovery

from translational repression. *EMBO J* **22:** 1180–1187. doi:10.1093/emboj/cdg112

Ohn T, Kedersha N, Hickman T, Tisdale S, Anderson P. 2008. A functional RNAi screen links O-GlcNAc modification of ribosomal proteins to stress granule and processing body assembly. *Nat Cell Biol* **10:** 1224–1231. doi:10.1038/ncb1783

Padrón A, Iwasaki S, Ingolia NT. 2019. Proximity RNA labeling by APEX-seq reveals the organization of translation initiation complexes and repressive RNA granules. *Mol Cell* **75:** 875–887.e5. doi:10.1016/j.molcel.2019.07.030

Pae C-U, Kim T-S, Kwon O-J, Artioli P, Serretti A, Lee C-U, Lee S-J, Lee C, Paik I-H, Kim J-J. 2005. Polymorphisms of heat shock protein 70 gene (HSPA1A, HSPA1B and HSPA1L) and schizophrenia. *Neurosci Res* **53:** 8–13. doi:10.1016/j.neures.2005.05.004

Paget M, Cadena C, Ahmad S, Wang H-T, Jordan TX, Kim E, Koo B, Lyons SM, Ivanov P, tenOever B, et al. 2023. Stress granules are shock absorbers that prevent excessive innate immune responses to dsRNA. *Mol Cell* **83:** 1180–1196.e8. doi:10.1016/j.molcel.2023.03.010

Pakos-Zebrucka K, Koryga I, Mnich K, Ljujic M, Samali A, Gorman AM. 2016. The integrated stress response. *EMBO Rep* **17:** 1374–1395. doi:10.15252/embr.201642195

Panas MD, Ivanov P, Anderson P. 2016. Mechanistic insights into mammalian stress granule dynamics. *J Cell Biol* **215:** 313–323. doi:10.1083/jcb.201609081

Panda AC, Martindale JL, Gorospe M. 2017. Polysome fractionation to analyze mRNA distribution profiles. *Bio Protoc* **7:** e2126. doi:10.21769/BioProtoc.2126

Pfaffl MW. 2001. A new mathematical model for relative quantification in real-time RT-PCR. *Nucleic Acids Res* **29:** e45. doi:10.1093/nar/29.9.e45

Popper B, Bürkle M, Ciccopiedi G, Marchioretto M, Forné I, Imhof A, Straub T, Viero G, Götz M, Schieweck R. 2024. Ribosome inactivation regulates translation elongation in neurons. *J Biol Chem* **300:** 105648. doi:10.1016/j.jbc.2024.105648

Putnam A, Thomas L, Seydoux G. 2023. RNA granules: functional compartments or incidental condensates? *Genes Dev* **37:** 354–376. doi:10.1101/gad.350518.123

Ren Z, Tang W, Peng L, Zou P. 2023. Profiling stress-triggered RNA condensation with photocatalytic proximity labeling. *Nat Commun* **14:** 7390. doi:10.1038/s41467-023-43194-2

Riback JA, Zhu L, Ferrolino MC, Tolbert M, Mitrea DM, Sanders DW, Wei M-T, Kriwacki RW, Brangwynne CP. 2020. Composition-dependent thermodynamics of intracellular phase separation. *Nature* **581:** 209–214. doi:10.1038/s41586-020-2256-2

Ripin N, Macedo de Vasconcelos L, Ugay DA, Parker R. 2024. DDX6 modulates P-body and stress granule assembly, composition, and docking. *J Cell Biol* **223:** e202306022. doi:10.1083/jcb.202306022

Rowlands AG, Panniers R, Henshaw EC. 1988. The catalytic mechanism of guanine nucleotide exchange factor action and competitive inhibition by phosphorylated eukaryotic initiation factor 2. *J Biol Chem* **263:** 5526–5533. doi:10.1016/S0021-9258(18)60596-4

Sage D, Unser M. 2001. Easy Java programming for teaching image-processing. In *Proceedings 2001 International Conference on Image Processing, Vol. 3*, pp. 298–301. IEEE, Thessaloniki, Hellenic Republic. doi:10.1109/ICIP.2001.958110

Sanders DW, Kedersha N, Lee DSW, Strom AR, Drake V, Riback JA, Bracha D, Eeftens JM, Iwanicki A, Wang A, et al. 2020. Competing protein-RNA interaction networks control multiphase intracellular organization. *Cell* **181:** 306–324.e28. doi:10.1016/j.cell.2020.03.050

Schindelin J, Arganda-Carreras I, Frise E, Kaynig V, Longair M, Pietzsch T, Preibisch S, Rueden C, Saalfeld S, Schmid B, et al. 2012. Fiji: an open-source platform for biological-image analysis. *Nat Methods* **9:** 676–682. doi:10.1038/nmeth.2019

Schneider C, Erhard F, Binotti B, Buchberger A, Vogel J, Fischer U. 2022. An unusual mode of baseline translation adjusts cellular protein synthesis capacity to metabolic needs. *Cell Rep* **41:** 111467. doi:10.1016/j.celrep.2022.111467

Schneider-Poetsch T, Ju J, Eyler DE, Dang Y, Bhat S, Merrick WC, Green R, Shen B, Liu JO. 2010. Inhibition of eukaryotic translation elongation by cycloheximide and lactimidomycin. *Nat Chem Biol* **6:** 209–217. doi:10.1038/nchembio.304

Scorsone KA, Panniers R, Rowlands AG, Henshaw EC. 1987. Phosphorylation of eukaryotic initiation factor 2 during physiological stresses which affect protein synthesis. *J Biol Chem* **262:** 14538–14543. doi:10.1016/S0021-9258(18)47829-5

Sharma V, Sood R, Khlaifia A, Eslamizade MJ, Hung T-Y, Lou D, Asgarihafshejani A, Lalzar M, Kiniry SJ, Stokes MP, et al. 2020. eIF2α controls memory consolidation via excitatory and somatostatin neurons. *Nature* **586:** 412–416. doi:10.1038/s41586-020-2805-8

Shin Y, Berry J, Pannucci N, Haataja MP, Toettcher JE, Brangwynne CP. 2017. Spatiotemporal control of intracellular phase transitions using light-activated optoDroplets. *Cell* **168:** 159–171.e14. doi:10.1016/j.cell.2016.11.054

Simsek D, Tiu GC, Flynn RA, Byeon GW, Leppek K, Xu AF, Chang HY, Barna M. 2017. The mammalian Ribo-interactome reveals ribosome functional diversity and heterogeneity. *Cell* **169:** 1051–1065.e18. doi:10.1016/j.cell.2017.05.022

Sinha NK, Ordureau A, Best K, Saba JA, Zinshteyn B, Sundaramoorthy E, Fulzele A, Garshott DM, Denk T, Thoms M, et al. 2020. EDF1 coordinates cellular responses to ribosome collisions. *eLife* **9:** e58828. doi:10.7554/eLife.58828

Smirnova AM, Hronová V, Mohammad MP, Herrmannová A, Gunišová S, Petráčková D, Halada P, Coufal Š, Świrski M, Rendleman J, et al. 2024. Stem-loop-induced ribosome queuing in the uORF2/ATF4 overlap fine-tunes stress-induced human ATF4 translational control. *Cell Rep* **43:** 113976. doi:10.1016/j.celrep.2024.113976

Spaulding EL, Hines TJ, Bais P, Tadenev ALD, Schneider R, Jewett D, Pattavina B, Pratt SL, Morelli KH, Stum MG, et al. 2021. The integrated stress response contributes to tRNA synthetase-associated peripheral neuropathy. *Science* **373:** 1156–1161. doi:10.1126/science.abb3414

Stöhr N, Lederer M, Reinke C, Meyer S, Hatzfeld M, Singer RH, Hüttelmaier S. 2006. ZBP1 regulates mRNA stability during cellular stress. *J Cell Biol* **175:** 527–534. doi:10.1083/jcb.200608071

Sun L, Tsai R, Yulyaningsih E, Fanok M, Vissers M, Heuberger J, Flores B, Huang F, Kane L, Cohen I, et al. 2023. The integrated stress response is modulated by eIF2B agonist DNL343: results from phase 1 healthy subject and phase 1b ALS patient studies. (P8-8.010). *Neurology* **100:** 3555. doi:10.1212/WNL.0000000000203354

Tang CP, Clark O, Ferrarone JR, Campos C, Lalani AS, Chodera JD, Intlekofer AM, Elemento O, Mellinghoff IK. 2022. GCN2 kinase activation by ATP-competitive kinase inhibitors. *Nat Chem Biol* **18:** 207–215. doi:10.1038/s41589-021-00947-8

Tauber D, Tauber G, Khong A, Van Treeck B, Pelletier J, Parker R. 2020. Modulation of RNA condensation by the DEAD-box protein eIF4A. *Cell* **180:** 411–426.e16. doi:10.1016/j.cell.2019.12.031

Tokunaga M, Imamoto N, Sakata-Sogawa K. 2008. Highly inclined thin illumination enables clear single-molecule imaging in cells. *Nat Methods* **5:** 159–161. doi:10.1038/nmeth1171

Tolay N, Buchberger A. 2021. Comparative profiling of stress granule clearance reveals differential contributions of the ubiquitin system. *Life Sci Alliance* **4:** e202000927. doi:10.26508/lsa.202000927

Tourrière H, Chebli K, Zekri L, Courselaud B, Blanchard JM, Bertrand E, Tazi J. 2003. The RasGAP-associated endoribonuclease G3BP assembles stress granules. *J Cell Biol* **160:** 823–831. doi:10.1083/jcb.200212128

Tsuchida K, Tsujita T, Hayashi M, Ojima A, Keleku-Lukwete N, Katsuoka F, Otsuki A, Kikuchi H, Oshima Y, Suzuki M, et al. 2017. Halofuginone enhances the chemo-sensitivity of cancer cells by suppressing NRF2 accumulation. *Free Radic Biol Med* **103:** 236–247. doi:10.1016/j.freeradbiomed.2016.12.041

Turakhiya A, Meyer SR, Marincola G, Böhm S, Vanselow JT, Schlosser A, Hofmann K, Buchberger A. 2018. ZFAND1 recruits p97 and the 26S proteasome to promote the clearance of arsenite-induced stress granules. *Mol Cell* **70:** 906–919.e7. doi:10.1016/j.molcel.2018.04.021

van Leeuwen W, VanInsberghe M, Battich N, Salmén F, van Oudenaarden A, Rabouille C. 2022. Identification of the stress granule transcriptome via RNA-editing in single cells and in vivo. *Cell Rep Methods* **2:** 100235. doi:10.1016/j.crmeth.2022.100235

Van Treeck B, Protter DSW, Matheny T, Khong A, Link CD, Parker R. 2018. RNA self-assembly contributes to stress granule formation and defining the stress granule transcriptome. *Proc Natl Acad Sci* **115:** 2734–2739. doi:10.1073/pnas.1800038115

Vattem KM, Wek RC. 2004. Reinitiation involving upstream ORFs regulates *ATF4* mRNA translation in mammalian cells. *Proc Natl Acad Sci* **101:** 11269–11274. doi:10.1073/pnas.0400541101

Wang B, Maxwell BA, Joo JH, Gwon Y, Messing J, Mishra A, Shaw TI, Ward AL, Quan H, Sakurada SM, et al. 2019. ULK1 and ULK2 regulate stress granule disassembly through phosphorylation and activation of VCP/p97. *Mol Cell* **74:** 742–757.e8. doi:10.1016/j.molcel.2019.03.027

Weber R, Wohlbold L, Chang C-T. 2024. Human DDX6 regulates translation and decay of inefficiently translated mRNAs. *eLife* **13:** RP92426. doi:10.7554/eLife.92426

Wek SA, Zhu S, Wek RC. 1995. The histidyl-tRNA synthetase-related sequence in the eIF-2α protein kinase GCN2 interacts with tRNA and is required for activation in response to starvation for different amino acids. *Mol Cell Biol* **15:** 4497–4506. doi:10.1128/MCB.15.8.4497

Whiffin N, Karczewski KJ, Zhang X, Chothani S, Smith MJ, Evans DG, Roberts AM, Quaife NM, Schafer S, Rackham O, et al. 2020. Characterising the loss-of-function impact of 5′ untranslated region variants in 15,708 individuals. *Nat Commun* **11:** 2523. doi:10.1038/s41467-019-10717-9

Wickham H. 2016. *Ggplot2, 2nd ed.* Springer International Publishing, Basel, Switzerland.

Wickham H, Averick M, Bryan J, Chang W, McGowan L, François R, Grolemund G, Hayes A, Henry L, Hester J, et al. 2019. Welcome to the tidyverse. *J Open Source Softw* **4:** 1686. doi:10.21105/joss.01686

Wisdom R, Johnson RS, Moore C. 1999. c-Jun regulates cell cycle progression and apoptosis by distinct mechanisms. *EMBO J* **18:** 188–197. doi:10.1093/emboj/18.1.188

Wong W, Bai X-C, Brown A, Fernandez IS, Hanssen E, Condron M, Tan YH, Baum J, Scheres SHW. 2014. Cryo-EM structure of the *Plasmodium falciparum* 80S ribosome bound to the anti-protozoan drug emetine. *eLife* **3:** e03080. doi:10.7554/eLife.03080

Yang P, Mathieu C, Kolaitis R-M, Zhang P, Messing J, Yurtsever U, Yang Z, Wu J, Li Y, Pan Q, et al. 2020. G3BP1 is a tunable switch that triggers phase separation to assemble stress granules. *Cell* **181:** 325–345.e28. doi:10.1016/j.cell.2020.03.046

Young SK, Wek RC. 2016. Upstream open Reading frames differentially regulate gene-specific translation in the integrated stress response. *J Biol Chem* **291:** 16927–16935. doi:10.1074/jbc.R116.733899

Young SK, Willy JA, Wu C, Sachs MS, Wek RC. 2015. Ribosome reinitiation directs gene-specific translation and regulates the integrated stress response. *J Biol Chem* **290:** 28257–28271. doi:10.1074/jbc.M115.693184

Zhang P, Fan B, Yang P, Temirov J, Messing J, Kim HJ, Taylor JP. 2019. Chronic optogenetic induction of stress granules is cytotoxic and reveals the evolution of ALS-FTD pathology. *eLife* **8:** e39578. doi:10.7554/eLife.39578

Zhang H, Wang Y, Wu X, Tang X, Wu C, Lu J. 2021. Determinants of genome-wide distribution and evolution of uORFs in eukaryotes. *Nat Commun* **12:** 1076. doi:10.1038/s41467-021-21394-y

Zhao C, Datta S, Mandal P, Xu S, Hamilton T. 2010. Stress-sensitive regulation of IFRD1 mRNA decay is mediated by an upstream open reading frame. *J Biol Chem* **285:** 8552–8562. doi:10.1074/jbc.M109.070920

Ribosome association inhibits stress-induced gene mRNA localization to stress granules

Noah S. Helton, Benjamin Dodd and Stephanie L. Moon

Genes Dev. published online May 13, 2025
Access the most recent version at doi:10.1101/gad.352899.125